Degree Project in Heat and Power Technology
Second cycle, 30 credits

Technoeconomic Analysis of Waste Heat Integration into District Heating Networks

Component-Level Analysis

JITHESH JAYARAM SREEDHAR

Master of Science Thesis

Department of Energy Technology

KTH 2026

Component-level Technoeconomic Analysis of Waste Heat Integration into District Heating Networks

Jithesh Jayaram Sreedhar

Approved	Examiner Jagruti Thakur	Supervisor Jagruti Thakur
TRITA: TRITA-ITM-EX 2026:602	Industrial Supervisor Fumi Bromander	Contact person Jagruti Thakur

Abstract

Swedish district heating is under growing cost pressure, with average prices rising 8 per cent in 2023 and a further 15.2 per cent the following year, driven largely by biomass fuel costs. Industrial waste heat offers a way to displace that fuel, yet of an estimated 22 TWh available annually in Sweden only around 29.5 per cent is currently recovered. The obstacle is not that sources are unknown, since mapping platforms identify them, but that deciding whether any particular source is worth connecting requires the connection itself to be designed and costed. Most existing work addresses waste heat at the system level, where district heating networks are represented in aggregate and individual connections are not resolved.

This thesis develops a component-level technoeconomic method for that decision and applies it consistently to four cases. Heat exchangers, heat pumps, connection pipes, circulation pumps and seasonal storage are each sized from the thermodynamic and hydraulic conditions of their own case, using CoolProp, TESPy and pandapipes across a full operating year at hourly resolution. The resulting levelised cost of heat is benchmarked against the avoided marginal production cost of the receiving network, following the prosumer framework of Energiforsk, and seasonal storage technologies are screened against the Danish Energy Agency operating conditions. The four cases span more than two orders of magnitude in annual heat volume and include both external network integration and recovery within a waste-to-energy plant.

The results show that connection distance together with the cost of any seasonal storage required and quantity of heat available prominently governs the viability. Supermarket refrigeration heat proved clearly unviable at 4,836 SEK/MWh against a 347 SEK/MWh benchmark, its cost dominated by a 3,500 m connection. An algae cultivation source 160 m from the network failed to clear benchmark cleared requiring a 128,775 m^3 store. A pulp mill managed to clear benchmark at 86.4 percent probability of viability by virtue of high waste heat available and the waste-to-energy plant returned outcome close to their thresholds at 41.3 per cent probability of viability. Within the plant, three small auxiliary streams recovered over 35 m delivered the cheapest heat in the study at 11.8 SEK/MWh, improving boiler efficiency by 0.95 percentage points without additional fuel. Because the method solves for a breakeven distance per source, it converts a case-specific result into a screening rule applicable to comparable sites of similar sources.

Sammanfattning

Svensk fjärrvärme står under ökande kostnadstryck, med genomsnittliga prisökningar på 8 procent under 2023 och ytterligare 15,2 procent året därpå, till stor del drivet av stigande biobränslekostnader. Industriell spillvärme erbjuder ett sätt att ersätta detta bränsle, men av de uppskattade 22 TWh som årligen finns tillgängliga i Sverige återvinns endast omkring 29,5 procent. Hindret är inte att källorna är okända, eftersom kartläggningsverktyg identifierar dem, utan att beslutet om huruvida en viss källa är värd att ansluta kräver att själva anslutningen dimensioneras och kostnadsberäknas. Merparten av befintlig forskning behandlar spillvärme på systemnivå, där fjärrvärmenät representeras aggregerat och enskilda anslutningar inte upplöses.

Detta examensarbete utvecklar en teknoekonomisk metod på komponentnivå för detta beslut och tillämpar den konsekvent på fyra fall. Värmeväxlare, värmepumpar, anslutningsledningar, cirkulationspumpar och säsongslager dimensioneras var för sig utifrån de termodynamiska och hydrauliska förhållandena i respektive fall, med hjälp av CoolProp, TESPy och pandapipes över ett helt driftår med timupplösning. Den resulterande utjämnade värmekostnaden jämförs med den undvikna marginella produktionskostnaden i mottagarnätet, enligt Energiforsks prosumentramverk, och säsongslagringstekniker utvärderas mot Danska Energimyndighetens driftförutsättningar. De fyra fallen spänner över mer än två tiopotenser i årlig värmemängd och omfattar både extern nätintegration och återvinning inom ett avfallsförbränningsverk.

Resultaten visar att anslutningsavståndet, tillsammans med kostnaden för erforderligt säsongslager och mängden tillgänglig värme, har en avgörande betydelse för lönsamheten. Spillvärme från en livsmedelsbutiks kylsystem visade sig vara tydligt olönsam, med en värmekostnad på 4 836 SEK/MWh jämfört med ett riktvärde på 347 SEK/MWh. Kostnaden dominerades av en anslutningsledning på 3 500 m. En spillvärmekälla från algodling, belägen 160 m från fjärrvärmenätet, nådde inte upp till riktvärdet eftersom den krävde ett lager med en volym på 128 775 m³. Ett massabruk uppnådde riktvärdet med en beräknad sannolikhet för lönsamhet på 86,4 procent, tack vare den stora mängden tillgänglig spillvärme, medan avfallsförbränningsanläggningen gav ett resultat nära sitt tröskelvärde, med en sannolikhet för lönsamhet på 41,3 procent. Inom anläggningen återvanns tre mindre hjälpvärmeströmmar över en sträcka på mer än 35 m och gav den lägsta värmekostnaden i studien, 11,8 SEK/MWh. Detta förbättrade pannans verkningsgrad med 0,95 procentenheter utan behov av ytterligare bränsle. Eftersom metoden löser ut ett brytpunktsavstånd per källa omvandlar den ett fallspecifikt resultat till en screeningregel tillämpbar på jämförbara anläggningar.

Acknowledgements

I would like to thank my supervisors at KTH and at Ramboll Sweden for their guidance throughout this work, and for the practical perspective that shaped the direction of the analysis. I am grateful to Patrik Selinder at Vattenfall for providing the network temperature profiles and measured operational data without which one of the four cases could not have been assessed, and to the engineering team at the waste-to-energy plant for their time, their process data, and their willingness to let an outside analysis be run on their operation.

I would also like to thank the fellow KTH student who shared the waste heat profile data used to construct the Case 3, and my supervisor for the review that improved this report.

Finally, I thank my family for their support and patience over the course of this thesis.

List of abbreviations

ATES	Aquifer thermal energy storage
BTES	Borehole thermal energy storage
CAPEX	Capital expenditure
CHP	Combined heat and power
COP	Coefficient of performance
CRF	Capital recovery factor
CTES	Cavern thermal energy storage
DEA	Danish Energy Agency
DH	District heating
DHN	District heating network
DN	Nominal pipe diameter
4GDH	Fourth generation district heating
HP	Heat pump
HX	Heat exchanger
LCOH	Levelised cost of heat
LHV	Lower heating value
LMTD	Logarithmic mean temperature difference
O&M	Operation and maintenance
OPEX	Operating expenditure
PTES	Pit thermal energy storage
SDG	Sustainable Development Goals
SMHI	Swedish Meteorological and Hydrological Institute
SOC	State of charge
TES	Thermal energy storage
TTES	Tank thermal energy storage
WH	Waste heat
WtE	Waste-to-energy

Table of Contents

Technoeconomic Analysis of Waste Heat Integration into District Heating Networks 1
Abstract 3
Sammanfattning 4
Acknowledgements 5
List of abbreviations 6
Table of Contents 7
1. Introduction 11
1.1 Background and motivation 11
1.1.1 District heating in Sweden 11
1.1.2 Waste heat as an underused resource 11
1.2 Sustainability Aspects 12
1.3 Structure of the thesis 12
2. Literature Review 13
2.1 District heating and its generations 13
2.2 Industrial waste heat: potential and characterisation 13
2.2.1 Scale of the resource 13
2.2.2 Temperature grade and its consequences 14
2.2.3 Source categories examined in this work 14
2.3 Connection components 15
2.4 Thermal energy storage 16
2.5 Technoeconomic assessment 16
2.6 The Research Gaps 17
2.6.1 The Assessment Gap: System-Level vs. Component-Level Assessment 17
2.6.2 The Scope Gap 17
3. Aim, Research Questions and Scope 19
3.1 Aim 19
3.2 Research questions 19
3.3 Scope 19
3.3.1 Inclusions 19

3.3.2 Exclusions 19
4. Case Studies 20
4.1 Case 1: ICA Maxi, Haninge — supermarket refrigeration 20
4.1.1 Site and source description 20
4.1.2 Host network and connection 20
4.1.3 Design space position 21
4.2 Case 2: AstaReal, Gustavsberg — algae cultivation auxiliary heat 21
4.2.1 Site and source description 21
4.2.2 Host network and connection 21
4.2.3 Design space position 22
4.3 Case 3: Metsä Board, Husum — kraft pulp mill process heat 22
4.3.1 Site and source description 22
4.3.2 Host network and connection 22
4.3.3 Design space position 23
4.4 Summary of the three cases 23
4.5 Case 4: Waste-to-Energy CHP Plant, Sweden — In-Plant Heat Recovery 24
4.5.1 Site and source description 24
4.5.2 Stream blending 25
4.5.3 Host network and connection 25
4.5.4 Design space position 25
4.6 Summary 26
5. Methodology 27
5.1 Overall framework 27
5.2 Software libraries and their roles 28
5.3 Input data and hourly profiles 28
5.3.1 Ambient temperature 28
5.3.2 District heating temperatures 29
5.3.3 Waste heat source characterisation 29
5.3.4 Stream combination 29
5.4 Component sizing 30
5.4.1 Heat pump 30
5.4.3 Pipe network optimisation 35

5.5 Thermal energy storage 37
5.6 Dynamic simulation 39
5.7 Economic evaluation 39
5.8 Sensitivity and uncertainty analysis 40
5.9 Plant Efficiency Evaluation 41
6. Results and Discussion 42
6.1 Case 1: ICA Maxi, Haninge 42
6.1.1 Key results & Component sizes 42
6.1.2 Dynamic simulation and Energy Losses 42
6.1.3 Pipe Diameter Optimisation 43
6.1.4 Levelised cost of heat and economic viability 44
6.1.5 Sensitivity and uncertainty 44
6.1.6 Discussion 45
6.2 Case 2: AstaReal, Gustavsberg 46
6.2.1 Component sizing 46
6.2.2 Dynamic simulation and Heat Loses 46
6.2.3 Pipe Diameter Optimisation 47
6.2.4 Thermal energy storage sizing and technology selection 47
6.2.5 Levelised cost of heat and economic viability 50
6.2.6 Sensitivity and uncertainty 50
6.2.7 Discussion 51
6.3 Case 3: Metsä Board, Husum 52
6.3.1 Component sizing 52
6.3.2 Dynamic simulation and heat losses 52
6.3.3 Pipe Diameter Optimisation 53
6.3.4 Thermal energy storage sizing and technology selection 53
6.3.5 Levelised cost of heat and economic viability 55
6.3.6 Sensitivity and uncertainty 55
6.3.7 Discussion 56
6.4 Case 4: Waste to Energy CHP Plant 57
6.4.1 Component sizing 58
6.4.2 Dynamic simulation and heat losses 58

6.4.3 Pipe diameter optimisation 59
6.4.4 Thermal energy storage sizing 60
6.4.5 Levelised cost of heat and economic viability 61
6.4.6 Sensitivity and uncertainty 63
6.4.7 Plant efficiency improvement 64
6.4.8 Discussion 66
7. Conclusions and Further Work 67
7.1 Answers to the research questions 67
7.2 The breakeven distance as a screening tool 68
7.3 Further work 68
References 70

1. Introduction

1.1 Background and motivation

1.1.1 District heating in Sweden

Space and water heating account for the largest single share of energy use in the European residential sector, exceeding 75 per cent of total residential demand (Eurostat, 2024). The way that heat is produced therefore has a correspondingly large influence on the emissions of the building stock. In Sweden the picture is more favourable than in much of Europe, largely because district heating became the dominant urban heating solution during the second half of the twentieth century. (Werner, 2017) Rather than each building operating its own boiler, heat is produced centrally and distributed as hot water through a buried pipe network, which allows fuels and heat sources that would be impractical at building scale, such as municipal waste, forest residues and industrial excess heat, to serve an entire town (Frederiksen and Werner, 2013).

District heating is not a stagnant technology. It has evolved through a sequence of generations, each characterised by lower distribution temperatures, better insulation and a wider range of admissible heat sources (Frederiksen and Werner, 2013). The systems operating in Sweden today are predominantly third-generation networks running at supply temperatures in the region of 70 to 100 °C, with a gradual movement towards the lower temperatures and more diverse supply mix associated with the fourth generation (Vlcan, 2025). This matters for the present work because the temperature at which a network operates determines directly which waste heat sources can be connected to it without additional upgrading.

The economic position of district heating has become less comfortable in recent years. Swedish district heating prices rose by an average of 8 per cent in 2023, which at the time was the steepest single-year increase since 1996 (Nils Holgersson-gruppen, 2023). However, this trend has accelerated drastically, with average prices surging by a record 15.2 per cent between 2023 and 2024. These severe price shocks are driven in large part by rising biomass fuel prices as demand for bio-based products grows in other sectors, exacerbated by supply chain disruptions (S&P Global Ratings, 2024). Operators face the prospect of losing customers to individual heat pumps, which in turn places pressure on electricity networks that are already constrained in many municipalities. Reducing the fuel consumed per unit of heat delivered is therefore not only an environmental objective but a commercial one as well.

1.1.2 Waste heat as an underused resource

Industrial processes reject large quantities of heat that serve no further purpose on site. In Sweden the technical potential of industrial excess heat is estimated at approximately 22 TWh per year, of which only around 29.5 per cent is currently recovered and delivered to district heating networks (Renström, 2025). The remainder is discharged to the atmosphere through cooling towers, stacks and heat exchangers. Recovering even a modest share of this would displace fuel that a network would

otherwise have to burn, which is the mechanism by which waste heat integration reduces both cost and emissions.

European policy recognises this potential explicitly. The Energy Efficiency Directive requires member states to assess waste heat potential as part of their heating and cooling planning (European Parliament and Council of the European Union, 2023), and the Fit for 55 package identifies excess heat integration into district heating as a priority measure for the sector (European Commission, 2021).

The reason so much of this resource remains unused is not that its existence is unknown. National and European mapping exercises, including the Hotmaps platform (Hotmaps, 2024) have identified candidate sites in considerable detail. The obstacle is that identifying a source tells you little about whether connecting it is worth doing. Renström, 2025, reviewing the barriers to waste heat recovery, find that the decisive obstacles are economic and organisational, the heat exists and can be captured, but the investment required to capture, upgrade and transport it must be justified against what the receiving network would otherwise have paid to generate the same heat.

A waste heat project is, in engineering terms, a piece of infrastructure. It requires a heat exchanger sized for the duty, a connection pipe of a particular diameter and length, a circulation pump able to overcome the pressure and transport the fluid, and in many cases a heat pump to raise the source temperature or a thermal store to bridge the gap between when heat is available and when the network can absorb it. Each carries a capital cost.

1.2 Sustainability Aspects

Waste heat recovery sits at the intersection of several sustainability targets rather than serving a single one. With reference to Sustainable Development Goals (SDG), it contributes directly to SDG 7 (affordable and clean energy) by displacing fuel that would otherwise be burned to produce the same heat, and to SDG 9 (industry, innovation and infrastructure) by making more productive use of energy that industrial processes already generate as a by-product rather than treating it as waste. It also supports SDG 13 (climate action), since every unit of recovered heat is a unit the district heating fleet does not need to produce by combustion. The European Green Deal and the Fit for 55 package, already noted in Section 1.1.2, translate these same priorities into binding European policy, with waste heat recovery identified explicitly as a measure the heating sector is expected to pursue (European Commission, 2021).

1.3 Structure of the thesis

Chapter 2 reviews the literature on district heating, the waste heat resource, connection components, thermal storage, technoeconomic assessment and the research gaps. Chapter 3 states the research questions, objectives and scope. Chapter 4 introduces the four case studies, Chapter 5 develops the methodology and its governing relations, and Chapter 6 presents and discusses the results case by case. Chapter 7 draws the conclusions and sets out recommendations for further work.

2. Literature Review

This chapter establishes the background against which the four cases are assessed. Section 2.1 traces the generations of district heating and explains why network temperature governs which sources can be connected. Section 2.2 reviews the scale and temperature grade of the industrial waste heat resource. Sections 2.3 and 2.4 summarise the literature on connection components and thermal storage; both are kept deliberately brief, since the governing equations, parameter values and sources used in this work are set out in full in Chapter 5 and applied in Chapter 6. Section 2.5 covers the technoeconomic frameworks used to judge whether a project is worth building and section 2.6 introducing the research gaps.

2.1 District heating and its generations

The standard reference on the different generations of district heating is Frederiksen and Werner (2013) and Vlcan (2025). The first generation, deployed in the United States from the 1880s, distributed steam at temperatures above 150 °C resulting in substantial heat losses. The second, dominant in Europe from the 1930s, used water instead of steam around or slightly over 100 °C reducing safety risk and reducing heat losses. The third generation, which came to prevail from the 1970s and remains the Swedish norm, distributes pressurised hot water at roughly 70 to 120 °C using pre-insulated bonded pipe, with return temperatures dropping as well to commonly in the range of 40 and 75 °C (Vlcan, 2025). Lower temperatures reduce distribution heat loss, improve the performance of any heat pumps connected to the network, and widen the range of sources whose heat is hot enough to be injected directly (Persson and Werner, 2012, Vlcan, 2025). The fourth generation, characterised by supply temperatures of roughly 50 to 70 °C with some literature exploring ultra-low supply temperatures as low as 35–45 °C. Then we have the final and fifth generation which has near ambient, ie 0-30 °C network temperatures effectively eliminating any thermal gradient.

This design shift has been enabled largely by technological advancements and the increased deployment of heat pumps capable of upgrading water to higher temperatures when needed. A key consequence of lowering network temperatures is the increased potential for waste heat integration, particularly low-grade waste heat, which had previously been unsuitable due to temperature limitations. This leads to larger potential for feasible use of heat sources such as geothermal, data centres, biomass CHP, and solar thermal energy. (Vlcan, 2025)

2.2 Industrial waste heat: potential and characterisation

2.2.1 Scale of the resource

For Sweden the technical potential of industrial excess heat is given as approximately 22 TWh annually against a utilisation rate of roughly 29.5 per cent (Renström, 2025). Broberg (2012) report that the industries actually delivering excess heat to Swedish district heating networks are led by pulp and paper, chemicals, steel and foundries, which reflects both the volumes involved and the temperatures at which those industries reject heat. At European level, Brückner (2015) reports that the largest

amounts of waste heat in industries are usually found in food and tobacco and pulp and paper, basic metals, chemical industry, and non-metallic minerals.

Spatially resolved inventories such as Hotmaps (2024) allow waste heat sites to be identified together with an estimate of available heat, its temperature and its proximity to existing network infrastructure by mapping the thermal demand densities across Europe. Kumar S (2025) extend this to a spatio-temporal optimisation of which urban excess heat sources a network should integrate and in what order. Such work characterises the resource and its system-level value; it does not size or cost an individual connection, which is the distinction developed in section 2.6.

2.2.2 Temperature grade and its consequences

Waste heat is conventionally classified by temperature, with low-grade heat commonly placed below about 100 °C, medium-grade between 100 and 400 °C, and high-grade above that (Jouhara, 2018). For district heating the relevant threshold is not absolute but relative. What matters is whether the source is hotter than the network water it must heat. The source temperature dictates the integration strategy. The logic is straightforward: if the waste heat temperature exceeds the network's supply temperature, it is injected directly into the supply line using a heat exchanger. If the temperature is lower than the supply requirement, the designer has two options: upgrade the temperature using a heat pump for supply-line injection, or inject the flow directly into the return line to pre-heat the water returning to the central plant (Dorotić, 2019). For instance, a stream at 100 °C from a pulp drying process can be injected directly into a supply main at 90 °C, whereas a stream at 40 °C from a refrigeration condenser sits below the network return temperature and cannot be injected at all without a heat pump to raise it and it will be further analysed in the cases introduced subsequently. For low-grade heat sources that are still warmer than the network's return water, injecting directly into the return line is often the more economical choice because it entirely avoids the high capital expenditure of a heat pump. (Wahlroos, 2018).

2.2.3 Source categories examined in this work

Supermarket refrigeration has been studied by Thanasoulas et al. (2023), who quantify the recoverable heat from a Swedish store of comparable size to the one examined here, and by Adrianto et al. (2018), who characterise the operating temperatures of transcritical CO_2 systems in Swedish conditions. Fricke (2011) provides the split of total condenser rejection between the desuperheater and the gas cooler, which determines the effective source temperature once the two streams are combined.

The second case involves a facility which cultivates Haematococcus pluvialis for the extraction of natural astaxanthin, with the cultivation taking place in closed photobioreactors that require space temperature to be maintained at 25 degrees. (Vattenfall Energy Plaza, 2022). The air-conditioning of the photobioreactors and downstream processing constitutes the waste heat source from the condenser side. The operational data required to analyse the case was supplied directly by the network operator as detailed in Section 4.2.

Pulp and paper mills are the one of the largest single category of Swedish industrial excess heat by volume (Broberg, 2012), and their process heat is rejected at temperatures well above network requirements. The source side heat quantity and temperature for the particular case studied is obtained using Hotmaps platform as detailed in Section 4.3.

Waste-to-energy plants occupy a different position again. They are themselves heat producers connected to a network, so the question is not whether to transport heat to a customer but whether heat currently lost within the plant is worth reclaiming. The auxiliary streams involved, such as soot blower drains, compressor aftercoolers and building services chillers, are generic to most thermal plants. The operational data and stream profiles for the plant examined in this thesis were shared directly by plant representatives and are treated as confidential as set out in Section 4.4.

2.3 Connection components

Bühler (2018) demonstrates that the comprehensive techno-economic evaluations of industrial heat recovery must individually size the heat exchangers and heat pumps based on source temperatures, while simultaneously sizing the transmission pipes and thermal storages. The design basis for each is well established, and the governing equations, parameter values and cost relations adopted in this work are set out in full in Chapter 5. This section therefore records only the sources from which those parameters are drawn.

Heat exchanger sizing follows the logarithmic mean temperature difference method of Incropera (2007) and Shah and Sekulić (2003). Overall heat transfer coefficients for water-to-water plate exchangers are taken from Engineering Toolbox (2003), and the substantially lower coefficient applicable to finned-tube gas-to-liquid heat exchanger from Bergman (2011); the two differ by roughly 100 times, which proves decisive for the air-sourced stream in the fourth case. Exchanger effectiveness in real industrial service is lower than clean design values suggest, and the range of 50 to 60 per cent reported by Vlcan (2025) for the Oskarshamn network is adopted here, as is the specific installed cost per unit area from the same source.

For heat pumps, natural refrigerants have displaced synthetic fluids in new district heating installations, and an isentropic compressor efficiency of 0.75 follows Sadowski (2022). Propane (R290) is selected as the refrigerant for the heat pump because it is a naturally occurring working fluid with an Ozone Depletion Potential (ODP) of zero and a negligible Global Warming Potential (GWP) (Bolaji, 2013).

Pipe diameter optimisation follows the trade-off set out by Frederiksen and Werner (2013). Pipe investment cost is taken as linearly proportional to the diameter while pumping cost falls as diameter increases through reduced frictional pressure drop, and minimising the sum of the two gives an optimal diameter. The velocity constraint applied in the present work and the linear heat-loss treatment for buried pre-insulated pipe are likewise drawn from Frederiksen and Werner (2013), with installed pipe

costs as a function of nominal diameter from nPro Technologies (2024) and pump efficiency from Pumps & Systems (2020).

2.4 Thermal energy storage

The authoritative reference for technology characteristics, dimensioning relations and costs is the Danish Energy Agency's Technology Data for Energy Storage, whose Chapter 140 covers pit (PTES), borehole (BTES), aquifer (ATES) and tank (TTES) storage (Danish Energy Agency and Energinet, 2018). Recovery efficiencies and the structural reasons behind the selection are compared by Baeuerle (2025).

The four concepts differ in the maximum temperature they can hold, charge and discharge speed, whether an auxiliary heat pump or buffer tank is required, the volumes at which they have been demonstrated, and the fraction of stored heat subsequently retrieved. These differences are what allow a technology to be selected rather than assumed, and the screening of each case against the DEA operating envelopes is carried out in Sections 6.2.4 and 6.3.4. Cavern storage sits outside the DEA screening but is relevant in the Swedish context, where several district heating caverns have been created by converting decommissioned oil storage cavities. The distinction between reusing an existing cavity and mining a new one is economically decisive, since excavation dominates the cost (Baeuerle, 2025).

2.5 Technoeconomic assessment

The levelised cost of heat is the standard metric for comparing heat supply options. It expresses total annualised cost, capital recovered over asset life at an assumed discount rate plus annual operating expenditure, divided by the heat actually delivered. Its appeal is that it reduces a project with several components of differing lifetimes to a single figure expressed in the same units as a heat price.

A levelised cost is only meaningful when compared. Comparing against the consumer tariff overstates the value of delivered heat, since the tariff carries network overhead, tax and margin that a prosumer's heat never displaces. Energiforsk (2022) instead frames the correct comparator around the concept of avoided cost, arguing that 'the avoided alternative that arises from receiving one kWh of heat from a prosumer is the cost of generating one extra kWh of heat elsewhere in the district heating grid,' and that accordingly 'the marginal generation cost per hour of district heating has to be used as a remuneration for the heat supplied by prosumers' in their own simulated case studies. This is the convention adopted throughout the present work. A project is judged viable if its levelised cost falls below what the network would otherwise have spent, at the margin, to produce the same heat itself.

Akar (2023), assessing a geothermal district heating scheme in Oklahoma, illustrate why the choice of comparator matters in practice. It reported levelised cost of heat across four production scenarios which is benchmarked directly against the natural gas price a household would otherwise pay. That comparator, the retail price a household currently pays, is appropriate to their question of whether geothermal heating is competitive with the customer's existing alternative, but it is not the comparator

that matters to a network operator deciding whether to accept a prosumer's heat, who is choosing between producing heat itself and buying it from an outside. The avoided marginal production cost is therefore the comparator adopted in this thesis.

In this thesis, the published consumer tariffs from which this marginal cost is derived for each network are taken from Vattenfall Värme AB (2024) for cases 1 & 2, and from Övik Energi (2026) for case 3.

2.6 The Research Gaps

This following section outlines the specific gaps in the current literature concerning industrial waste heat integration that this thesis aims to address.

2.6.1 The Assessment Gap: System-Level vs. Component-Level Assessment

Most existing waste heat studies and spatial mapping platforms, identify heat recovery potential strictly at a macro level. These system-level approaches typically utilize tools like OSeMOSYS or EnergyPLAN to focus on whole energy-system optimization as demonstrated by by Kumar (2025) in their spatio-temporal optimization of urban excess heat. The primary strengths of these macro-level studies lie in strategic planning and policy development, yielding outputs related to broad capacity expansion and optimal dispatch. However, while such work characterizes the macro-resource and its systemic value, it fundamentally stops short of sizing or costing individual components for the waste heat integration.

This creates a critical gap between macro planning and actual engineering feasibility. To determine if a specific integration project is practically and economically viable, it must be evaluated at the component level to output precise design metrics such as pipe size, pump power, heat exchanger (HX) area, and the heat pump capacity. While authors like Bühler (2018) have demonstrated the necessity of individual component sizing and costing, this thesis bridges the gap further by shifting the analytical focus directly to the feasibility of single connections. By employing component-level engineering tools like TesPy and Pandapipes, this work provides the high engineering detail per project that macro-models lack.

2.6.2 The Scope Gap

While individual component-level case studies of waste heat do exist in the literature, they frequently assess a single type of source in isolation such as Thanasoulas (2023) focusing exclusively on supermarket refrigeration. This thesis addresses this gap by analysing highly contrasting cases that span the practical design space in several dimensions:

1. **Orders of Magnitude in Heat Volume:** This work contrasts annual waste heat capacities varying by more than two orders of magnitude, ranging from a 1,090 MWh/yr commercial source to a 179,000 MWh/yr industrial source.
2. **Varying Connection Distances:** This study tests the economic limits of piping infrastructure by comparing connection distances ranging from a few meters to an extended 3,500 meters.

3. **External Integration vs. In-Plant Recovery:** The dominant focus of waste heat integration literature is the transportation of external industrial heat from prosumers to a municipal network. Internal recovery mechanisms within the plant are largely ignored outside of major interventions like flue gas condensation covered by Bocchio, 2017. This work expands that traditional scope by including in-plant heat recovery streams where the source and sink share an operator and connection distances shrink to tens of meters.

By systematically evaluating these extremes in temperature, distance, and scale of heat, this work moves beyond establishing whether a single project is feasible, to identifying the thresholds that govern waste heat viability across different sectors.

3. Aim, Research Questions and Scope

3.1 Aim

The aim of this thesis is to carry out component-level technoeconomic analysis for assessing whether a given industrial waste heat source is worth connecting to a district heating network, and to apply it consistently across four contrasting cases in order to establish which design variables govern project viability.

3.2 Research questions

The work is organised around two research questions.

RQ1. What component sizes and specifications are required to make each waste heat integration technically feasible?

RQ2. What is the levelised cost of the delivered waste heat in each case, and does it fall below the marginal production cost of the receiving district heating network?

3.3 Scope

3.3.1 Inclusions

The geographical scope covers waste heat sites, district heating plant and networks within Sweden. The analysis covers the connection infrastructure between the waste heat source and the point of injection into the district heating network: the heat exchanger, the heat pump where the source temperature requires one, the connection pipework, the circulation pump, and seasonal thermal storage. Each is sized from the thermodynamic and hydraulic conditions of its own case. Scope also includes the economic evaluation of the connection over its full lifetime; the dynamic simulation of the package at hourly resolution for one full calendar year representative of the operating conditions.

3.3.2 Exclusions

The following are explicitly excluded from the scope: detailed mechanical design of the components below the level required for cost estimation (e.g., compressor selection, motor selection, tube bundle layout). The civil and structural design of trenches and chambers beyond the use of standard installed cost data is out of scope. Pipe connection distances are estimates from mapping rather than surveyed alignments. Financial and the contractual structure of any heat purchase agreement are not addressed.

4. Case Studies

The case studies are introduced in this chapter at the descriptive level here, with the technical and economic results developed in subsequent chapters once the methodology has been presented in Chapter 5. The three cases were selected to include representation across four dimensions: connection distance from source to network, annual waste heat content, source temperature relative to the network operating regime, and the temporal profile of source heat availability through the year ranging from near-continuous output to sources subject to planned seasonal shutdowns.

4.1 Case 1: ICA Maxi, Haninge — supermarket refrigeration

4.1.1 Site and source description

ICA Maxi Haninge is a large-format supermarket located in Haninge municipality, Stockholm County, approximately 25 km south of the Stockholm city centre. The store has a floor area of approximately 11,000 m², which matches the ICA Maxi store in Stenhagen, Uppsala studied by Thanasoulas (2023); this size equivalence was confirmed through Google Earth and forms the basis for transferring the waste heat characterisation from the study to the Haninge site.

The store operates a transcritical CO_2 refrigeration system serving medium-temperature display cabinets and low-temperature frozen cabinets. The system rejects heat through two streams: a desuperheater and a dry cooler (gas cooler). The temperature of the streams are 68 °C at the desuperheater outlet and 30 °C at the dry cooler outlet which is further supported by a separate study on CO_2-based supermarket refrigeration systems in Sweden by Adrianto (2018). The heat duty split between the two streams follows Fricke (2011), who reports that the dry cooler carries approximately 74 % of total condenser rejection while the desuperheater accounts for the remaining 26 %. Taking the weighted average across both streams gives an effective source temperature of approximately 40 °C.

Since this weighted average temperature falls below the average DHN return temperature, direct heat exchange to the network is not thermodynamically feasible and a heat pump is required to upgrade the waste heat to a network-compatible delivery temperature. The total annual heat rejection is taken as 1,090 MWh/yr at constant output, reflecting the fact that supermarket refrigeration systems operate continuously throughout the year regardless of season.

4.1.2 Host network and connection

The supply and return temperatures of the host network are taken in line with the Vattenfall and SamEnergi network temperature profiles for the Gustavsberg area, shared directly by Patrik Selinder at Vattenfall (P. Selinder, Vattenfall 2026) as a function of ambient temperature and consistent with the Swedish national average reported by Frederiksen and Werner (2013). The connection distance from the supermarket to the nearest district heating main is approximately 3,500 m, measured along the road pattern on Google Earth, reflecting the location of the store relative to the network.

The marginal production cost of the host network is taken as 347 SEK/MWh, derived from the Prisändringsmodell for Haninge, Tyresö, Älta och Gustavsberg (2024). The consumer price range published in that document was averaged across summer and winter tariffs and then multiplied by a factor of 0.7 to strip out taxes, profit margins, and other overheads, leaving the underlying marginal production cost as the economic benchmark for this case. The calculation of the marginal production cost is further detailed in chapter 5.7.

4.1.3 Design space position

The ICA Maxi case occupies the lower end of the design space defined by low source temperature, low annual volume, and long connection distance. It is included as a test of the methodology's ability to characterise the conditions under which low-grade heat is unviable for network integration. The case is also relevant beyond the specific site because supermarkets are a large and spatially distributed source category in Sweden, with over 900 ICA Maxi stores nationally; the conclusions for ICA Maxi Haninge are indicative for the broader category.

4.2 Case 2: AstaReal, Gustavsberg — algae cultivation auxiliary heat

4.2.1 Site and source description

AstaReal AB operates an algae cultivation facility in Gustavsberg, Värmdö municipality, approximately 20 km east of Stockholm city centre. The facility cultivates Haematococcus pluvialis for the extraction of natural astaxanthin, with the cultivation taking place in closed photobioreactors that require space temperature to be maintained at 25 degrees. (Vattenfall Energy Plaza, 2022). The air-conditioning of the photobioreactors and downstream processing constitutes the waste heat source from the condenser side.

The annual delivered heat is taken as 14,657 MWh/yr, measured directly by the host network at the cold side of the heat exchanger. The supply temperature is in the range 77–105 °C and the network return temperature is in the range 40–52 °C with annual variation reflecting consumer extraction patterns. All above data and hourly data for the 2025 calendar are provided by Patrik Selinder at Vattenfall and is the primary source for the dynamic simulation of this case. (P. Selinder, Vattenfall, 2026)

4.2.2 Host network and connection

The host network is the SamEnergi district heating system in Gustavsberg, which is operated under a service agreement by Vattenfall. SamEnergi is a smaller utility than the main Vattenfall Stockholm network. The marginal production cost for SamEnergi is derived from Prisändringsmodell for Haninge, Tyresö, Älta och Gustavsberg (2024).

The connection from the AstaReal site to the SamEnergi supply main is 160 meter as confirmed by Patrik. (P. Selinder, Vattenfall 2026)

4.2.3 Design space position

The AstaReal case occupies the corner of the design space defined by moderate source temperature, high annual waste heat capacity, short connection distance with annual shutdown. The availability of measured hourly network and heat source data is a substantial methodological advantage here.

4.3 Case 3: Metsä Board, Husum — kraft pulp mill process heat

4.3.1 Site and source description

Metsä Board operates a fully integrated kraft pulp and board mill at Husum, Örnsköldsvik municipality, in northern Sweden. Husum mill has two board machines with a production capacity of 400,000 tonnes of folding boxboard and 250,000 tonnes of white kraftliner a year. The mill can produce 730,000 tonnes of chemical pulp a year. (Packaging Gateway, 2023)

The waste heat source for the present analysis is the process heat rejected from the pulp drying and evaporation stages, characterised by source temperatures in the range 100–200 °C with an annual average of approximately 150 °C. The annual recoverable waste heat at the source side of the integration heat exchanger is taken as 179,000 MWh/yr, sourced from the Hotmaps platform (Hotmaps, 2024) for the Husum site. After the integration heat exchanger with effectiveness ε = 0.55, approximately 98,450 MWh/yr is delivered to the host network supply line. The Metsä Board waste heat profile presents a particular challenge, as no operational data could be obtained directly from the mill. To construct a physically representative hourly profile, waste heat enthalpy values from a comparable cardboard manufacturing facility were used as the basis. These values were shared by a fellow KTH master's student from their own thesis work, on the condition that the underlying source remain undisclosed. The data provided the characteristic magnitude and temporal shape of process waste heat, which was then scaled to match the annual waste heat availability reported for the Husum site.

4.3.2 Host network and connection

The host network is the Övik Energi district heating system serving Örnsköldsvik. Övik Energi is a medium-sized Swedish municipal. The Övik Energi DHN supply curve was modelled as a linear function following (P. Selinder, Vattenfall 2026), calibrated to northern Swedish ambient conditions: 110°C at −20°C ambient declining linearly to 80°C at +5°C and above. Return temperatures were set at 55°C (peak winter) and 45°C (peak summer). In the absence of a published Övik Energi supply temperature curve, the network was modelled using a linear curve of the same functional form as the Stockholm network (P. Selinder, Vattenfall 2026).

The marginal production cost for Övik Energi is taken as 263.2 SEK/MWh, computed from the operator-published consumer prices, Övik Energis prisändringsmodell (2026). The connection distance from the Husum mill to the Övik Energi supply main is approximately 900 m, estimated from the google maps using district heating demand density map for Örnsköldsvik from Hotmaps.

4.3.3 Design space position

The Metsä Board case occupies the corner of the design space defined by high source temperature, high waste heat capacity, moderate connection distance with seasonal shutdown. The case is of practical importance because paper and pulp mills are among the leading excess waste heat category in the Swedish industrial sector by volume. (Lygnerud and Werner, 2012)

4.4 Summary of the three cases

Taken together, the three case studies sample the design space at three points that differ by more than two orders of magnitude in annual volume, by more than a factor of three in source temperature, and by more than a factor of twenty in connection distance. They also sample different host network operators with different marginal cost benchmarks, different DHN supply temperatures, and different network sizes. The conclusions drawn from the three cases, when combined with the consistent methodology applied across them, support decision criteria that drive project viability.

Table 4.1. *Overview of the three case studies and their position in the design space.*

Attribute	ICA Maxi, Haninge	AstaReal, Gustavsberg	Metsä Board, Husum
Source type	CO_2 supermarket refrigeration	Algae cultivation auxiliary heat	Pulp mill process heat
Classification in design space	Low temperature, low heat, long distance, continuous heat source	Moderate temperature, high heat, low distance with annual shutdown	High temperature, high heat, long distance with annual shutdown
Annual heat available(MWh/yr)	1,090	14,657	179,000
Source temperature (°C)	40 (weighted average)	70–75	100–200
Host DHN operator	Vattenfall (Stockholm)	SamEnergi / Vattenfall	Övik Energi (Örnsköldsvik)
Connection distance (m)	3,500	160	900
Heat pump required for heat upgrade	Yes (R290)	No	No
Injection point	DHN return	DHN return	DHN supply
Source profile	constant 24×7	Real Vattenfall hourly data	Synthesized based on industrial data
TES required	No	Yes	Yes

4.5 Case 4: Waste-to-Energy CHP Plant, Sweden — In-Plant Heat Recovery

Note: at the plant's request, the facility and district heating utility providers are anonymised throughout. The plant is referred to as the XYZ boiler at a municipal waste-to-energy CHP facility in Sweden.

4.5.1 Site and source description

The fourth case departs from the pattern of the preceding three. Where Cases 1 to 3 examine heat leaving an industrial site and travelling to a district heating network, this case turns the same component-level method inward, to heat lost within the boundary of a district heat producing plant itself. The distinction matters methodologically: the source and the sink belong to the same operator, the connection distances reduce from kilometres to a few tens of metres, and the question shifts from whether external heat is worth transporting to whether internal waste heat are worth reclaiming and evaluating the improvement in the plant's boiler efficiency.

The facility is a municipal waste-to-energy combined heat and power plant operating a 70 MW boiler, designated XYZ, which combusts approximately 25 t/h of municipal solid waste with a lower heating value between 9.5-11 MJ/kg MJ/kg. Steam is raised at 420 °C and 45 bar and expanded through a turbine for electricity generation, with the turbine exhaust condensed against the district heating circuit. The plant already operates at a high thermal utilisation by design, with a stated boiler efficiency of 0.93 on the steam-output boundary. The losses are dispersed across various heat streams within the plant, which could be recovered at a negligible transport cost since they are located within a short distance from the network connection.

Four recoverable streams were identified through systematic review of the plant's process screens and a year of daily operational data, following consultation with the engineering team in the plant.

Soot blower drain (HS-4). The soot blowing system periodically injects steam to clear ash deposits from boiler tube surfaces, and the resulting drain water is routed to the bottom blowdown tank. The drain carries approximately 350 kW at an average temperature of around 58 °C, amounting to 2,800 MWh/yr. The temperature profile has not yet been metered continuously in this case. The flow is known to be within a range of 2 to 12 m^3/h, with a mid-range value of 7 m^3/h adopted here.

Compressor aftercooler (HS-8). Instrument air compression rejects heat through an aftercooler, with the cooling air rising from 26 °C to 174 °C while the compressed air is cooled from 179 °C to 31 °C. Accounting for the compressor duty cycle, the recoverable duty is 145 MWh/yr. With air being the cooling medium here, it is by a wide margin the smallest stream in the study, but it is also the only one at a temperature high enough for supply-side injection.

Chiller condenser (HS-9). The water-cooled chiller serving the plant's control rooms rejects 290 kW at its condenser, with the condenser fluid leaving at 42 °C at a flow of 11.2 l/s. Operating whenever ambient temperature exceeds 0 °C, the stream delivers approximately 1,595 MWh/yr.

Cooling tower summer surplus (HS-10). In summer, boiler output routinely exceeds what the district heating network can absorb, and the excess is rejected through the plant's cooling towers. Measured rejection totals approximately 25,500 MWh/yr. Unlike the three streams above, this is not a thermodynamic loss to be recovered by a heat exchanger; it is already-produced heat that the network cannot receive at the moment it is available. It is therefore treated as a seasonal storage question rather than a recovery question, and its treatment is developed separately in the results.

4.5.2 Stream blending

The three continuous streams differ in both temperature and medium, and this drives the connection architecture. The soot blower drain at 58 °C and the chiller condenser at 42 °C are both water based and both low-grade; the chiller condenser alone sits below the network return temperature of approximately and cannot be injected in isolation. Combining the two into a single recovered-water loop resolves this: the heat-weighted average temperature of the combined stream, computed as

$$T_{\text{combined}} = \frac{\sum Q_i T_i}{\sum Q_i}$$

sits comfortably above the return temperature, so that the warmer soot blower stream effectively lifts the cooler chiller stream into a usable range. This is the same weighted-average logic applied in Case 1 to the desuperheater and dry cooler streams at ICA Maxi, though with a different outcome: there, the weighted average fell below the return temperature and a heat pump became necessary, while here the blend clears the threshold and direct exchange is possible.

The compressor aftercooler is kept on a separate circuit. Its cooling medium is air rather than water, so no physical mixing is possible upstream of a heat exchanger.

4.5.3 Host network and connection

The host network is the municipal district heating system supplied by the same plant, which massively reduces the heat transport question that dominates Cases 1 and 3. The operator estimates the required new connection pipework at 30 to 40 m in total for all identified streams. The network operates with an average supply temperature of approximately 76 °C and a return temperature averaging 46 °C.

The marginal production cost benchmark for this case was provided directly by the plant, on the condition that the underlying tariff figures remain confidential. This differs procedurally from Cases 1 to 3, where the benchmark was derived from published consumer price documents. Here, the plant supplied the resulting marginal cost directly.

4.5.4 Design space position

This case occupies a corner of the design space that the first three do not reach: very short connection distance, high total annual heat volume, and a source temperature of the waste heat streams range

spanning both below-return and above-supply network conditions. It is also the only case in which source and sink share an owner, which removes the commercial negotiation and reduces the analysis to a purely internal investment decision.

The case is of broader relevance because waste-to-energy plants are a substantial and growing category in the Swedish district heating system, and because the streams examined here, soot blower drains, compressor aftercoolers, and building services chillers, are generic auxiliary systems present in almost any thermal plant. The conclusions are therefore indicative for in-plant recovery across the wider category rather than specific to this facility.

A further feature distinguishes this case from the preceding three. Because the recovered streams add useful output without consuming additional fuel, their effect can be expressed as a change in plant efficiency as well as in cost terms. This provides a second evaluation metric alongside LCOH.

4.6 Summary

The case studies span four host network operators with distinct marginal cost benchmarks, and they include both external prosumer integration and internal plant recovery. The addition of the fourth case extends the study from the question of whether waste heat should be transported to a network, to the question of whether the waste heat should be lost at all within the plant that produces the network's heat and the extent to which the plant’s efficiency could be improved.

5. Methodology

This chapter sets out the technoeconomic method used to assess the waste heat integration cases introduced in Chapter 4. The guiding principle is consistent: a single simulation method, built in Python around a small set of open-source engineering libraries, is applied to all the cases.

The method departs from the steady-state, design-point. Instead of collapsing a year of operation into a single representative hour, the framework simulates all 8,760 hours of the year, evaluating the thermodynamic and hydraulic state of the connection at each hour from measured or literature-derived source and weather data. This dynamic treatment is what allows the analysis to capture seasonal effects. For example, a heat pump whose COP drifts with ambient temperature and a connection pipe whose heat loss varies with the season.

5.1 Overall framework

The source is first characterised as an hourly profile of heat availability and temperature. The network operating temperatures are then established as functions of ambient conditions. From these, the heat exchanger is sized along with the heat pump where required. The connection pipe diameter is then optimised for lowest cost, the booster pump sized against the resulting hydraulics, and thermal storage sized. Finally, the levelised cost of heat is evaluated and benchmarked against the host network's marginal production cost, with the verdict tested through sensitivity and Monte Carlo analysis.

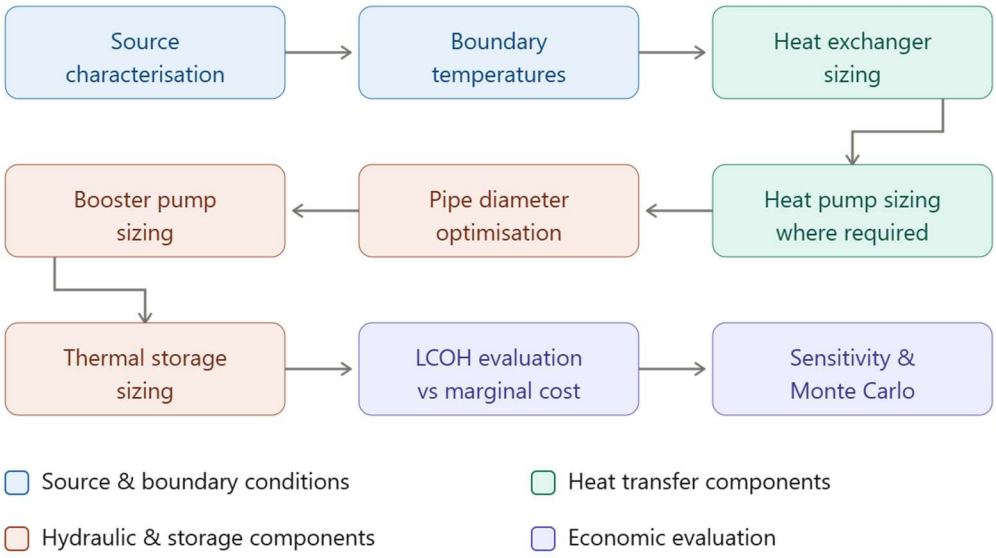

Figure 5.1. *Calculation sequence, from source characterisation through component sizing to the economic verdict.*

The sequence is executed once per case. Its individual stages are developed in the sections that follow: the software libraries and their roles (Section 5.2), the input data and hourly profiles (Section 5.3), the stream combination (Section 5.4.1), the component sizing models with their governing equations

(Section 5.4), the dynamic simulation (Section 5.5), thermal storage (Section 5.6), and the economic evaluation, sensitivity analysis and Monte Carlo simulation (Sections 5.7 and 5.8) , and the plant efficiency evaluation applied to the in-plant case (Section 5.9).

Case 4 departs from this single-source pattern in a few aspects. First, it comprises multiple parallel waste heat streams rather than a single source, so the component sizing are executed once per stream. Second, because the source and the sink share an operator and a defined efficiency boundary, the case admits a second evaluation metric alongside the levelised cost which is the evaluation of the improvement in the efficiency of the plant boiler. For Case 4 the calculation sequence of Figure 5.1 is therefore executed in parallel branches, one per stream, converging at the economic evaluation

5.2 Software libraries and their roles

The framework is implemented in Python and relies on a small number of established open-source libraries.

- **CoolProp** supplies the real thermophysical properties of water and of the R290 refrigerant in the heat pump design. Density, specific heat capacity and dynamic viscosity are evaluated at the actual temperature and pressure of each hour. For Case 4, CoolProp is additionally used to evaluate the properties of air, required for the energy balance across the air-cooled compressor aftercooler stream.
- **TESPy** (Thermal Engineering Systems in Python) solves the the complete vapour-compression heat pump cycle, as a network of mass and energy balances. This replaces Carnot-efficiency assumption using real refrigerant properties.
- **pandapipes** provides an independent hydraulic check on the selected pipe, solving the Colebrook–White friction to calculate pressure drop due to friction for sizing circulation pumps.

5.3 Input data and hourly profiles

The site-level description of each waste heat source, together with the host network's supply and return temperature, connection distance, and marginal production cost, is set out in Chapter 4 and is not repeated here. This section instead describes how those quantities were converted into the hourly time series that drive the dynamic simulation and the data sources used.

5.3.1 Ambient temperature

Ambient temperature drives the network heat curve. For the two Stockholm-area cases it is taken from measured hourly SMHI data for the 2025 calendar year at station 98230, Stockholm-Observatoriekullen A, comprising 8,758 measured hours with two missing values filled by linear interpolation. For Metsä Board the corresponding measured SMHI record for Örnsköldsvik is used, reflecting the colder northern climate in which Övik Energi operates. For case 4, the daily profile of the ambient temperature is provided by the plant representatives.

5.3.2 District heating temperatures

The network supply and return temperatures reported in Chapter 5 are the linear function of ambient temperature, constructed following data from Vattenfall (P. Selinder, Vattenfall 2026) and verified against Frederiksen and Werner (2013) for Swedish averages. At each hour of the simulation, the ambient temperature described in Section 5.3.1 is mapped through this function to obtain the corresponding supply and return temperature. This framework allows the network temperature to vary realistically through the year. For Case 4 the network supply and return temperatures are taken directly from the plant's own operational record.

5.3.3 Waste heat source characterisation

The way each source is characterised follows from the nature of its underlying process, and the four differ materially in how the hourly profile was obtained as given in Chapter 4. For ICA Maxi, the annual heat quantity and source temperature are treated as constant through the year since the desuperheater along with the dry cooler is assumed to sit indoors in the refrigeration plant room, and its rejection is governed by the store's internal cooling load rather than by the weather. Also the refrigerant load within the conditioned supermarket space is assumed to be constant and hence remain unchanged at every hour. For AstaReal, the real measured hourly heat-delivery data supplied by Vattenfall (P. Selinder, Vattenfall 2026) for the 2025 operating year are used directly as the hourly profile, capturing the actual seasonal and maintenance-driven variability of the algae process without any synthetic reconstruction.

Unlike AstaReal, no operational hourly data could be obtained directly from the Husum mill. The construction of a representative hourly profile for this case included the use of enthalpy data from a comparable, confidentially-sourced facility and its scaling to the Husum annual total is described in Section 4.3.1.

For Case 4, the plant supplied a full operating year of process data at daily-average resolution rather than hourly. All time-series calculations for this case are performed on a 365-point daily series rather than an hourly one. The four streams differ in the completeness of their characterisation. The cooling tower rejection stream is measured directly by the plant's own instrumentation across the full operating year. The chiller condenser stream is characterised from the manufacturer's datasheet with the flow and temperature of the cooling stream for the water-cooled condenser provided. The soot blower drain and compressor aftercooler streams are characterised from design-point temperatures with flow rates known only as ranges and mid-range values adopted.

5.3.4 Stream combination

This section generally applies to Case 1 and Case 4, in which multiple parallel streams are available within a single plant boundary. Where several streams are available, two questions precede exchanger

sizing: which streams may be physically combined, and whether each resulting stream could be injected into the network.

Combination is governed first by the medium. Streams sharing a common medium may be brought together into a single recovery loop upstream of one exchanger. Streams of differing media cannot be physically mixed and require separate exchangers regardless of their relative temperatures. Where streams are combined, the temperature of the resulting mixed stream is the heat-weighted average of its constituents:

$$T_{combined} = \frac{\sum Q_i T_i}{\sum Q_i} \quad (5.1)$$

where Q_i and T_i are the duty and temperature of the i-th constituent stream.

This combination logic is the same as that applied to the two condenser streams in Case 1, where the desuperheater and dry cooler rejection were combined by the same weighting to obtain an effective source temperature. The combination of a warmer and a cooler stream produces a resultant mixed temperature which if found to be greater than network temperature , a heat pump installation for upgrading waste heat could be excluded.

5.4 Component sizing

5.4.1 Heat pump

The heat pump was sized using a full thermodynamic model of its refrigeration cycle, built with the open-source Python library TESPy (Thermal Engineering Systems in Python). This approach solves the mass and energy conservation equations at each component simultaneously and yields a physically consistent set of state points from which the coefficient of performance emerges as a result.

The working fluid selected was R290 (propane), a natural refrigerant with negligible global warming potential and ozone depletion potential. Real fluid properties for both R290 and water were evaluated throughout using the CoolProp property library.

The heat pump was represented as a vapour compression cycle comprising four thermodynamic processes: evaporation of the refrigerant while absorbing heat from the waste heat stream, compression to the condensing pressure, condensation while rejecting heat to the district heating stream, and isenthalpic expansion back to the evaporating pressure. The refrigerant circuit was closed by a cycle-closer element enforcing overall mass and energy conservation, and coupled to two external water streams representing the waste heat source and the district heating network.

The evaporating temperature was set below the waste heat source temperature by a fixed approach temperature, providing the temperature difference necessary to drive heat transfer across the evaporator:

$$T_{evap} = T_{src} - \Delta T_{app,wh} \qquad (5.2)$$

Where T_{evap} is the evaporator temperature and T_{src} is the temperature of the waste heat source. An approach of $\Delta T_{app,wh} = 5\text{K}$ was applied consistent with the value adopted by Adrianto (2018) in the equivalent CO_2 transcritical supermarket refrigeration case. The waste heat stream was permitted to cool only to a temperature slightly above the evaporating temperature, preventing a temperature cross within the exchanger:

$$T_{wh,out} = T_{evap} + \Delta T_{app,hx} \qquad (5.3)$$

On the condenser side, an analogous approach temperature governs the relationship between the condensing temperature and the district heating return temperature. Rather than fixing the condensing temperature at a single design-point value throughout the year, a floating condenser control scheme was adopted, in which the condenser temperature is permitted to track the prevailing district heating return temperature, thus enabling the heat pump to function at a higher COP during the summer months:

$$T_{cond} = T_{ret,DH} + \Delta T_{app,DH} \qquad (5.4)$$

Governing conservation equations

At steady state, each component of the cycle must satisfy conservation of mass and energy. Mass conservation requires that, for each stream passing through a component, the mass flow entering equals the mass flow leaving:

$$\sum \dot{m}_{in} = \sum \dot{m}_{out} \qquad (5.5)$$

Since the refrigerant circuit is a closed loop without branching, the same refrigerant mass flow rate circulates through every component.

$$\dot{Q}_{evap} = \dot{m}_{ref}\left(h_{ev,out} - h_{ev,in}\right) \qquad (5.6)$$

Energy conservation for each component takes the general steady-flow form

$$\sum \dot{m}_{in} h_{in} = \sum \dot{m}_{out} h_{out} + \dot{W} \qquad (5.7)$$

where h denotes specific enthalpy and $\dot{W}$ the shaft work, which is zero for the heat exchangers and the expansion valve and $\dot{W} = \dot{W}_{comp}$ for the compressor.

Component-specific relations

The compressor was characterised by its isentropic efficiency, defined as the ratio of the ideal enthalpy rise under isentropic compression to the actual enthalpy rise:

$$\eta_s = \frac{h_{2s} - h_1}{h_2 - h_1} \qquad (5.8)$$

where h_1 is the enthalpy at the compressor inlet, h_2 the actual enthalpy at the outlet, and h_{2s} the enthalpy that would result from isentropic compression to the same discharge pressure. Rearranging gives the actual discharge enthalpy,

$$h_2 = h_1 + \frac{h_{2s} - h_1}{\eta_s} \qquad (5.9)$$

and the compressor power follows from

$$\dot{W}_{comp} = \dot{m}_{ref}(h_2 - h_1) \qquad (5.10)$$

Isentropic efficiency of of $\eta_s = 0.75$ was applied consistent with a heat pump modelling study (Sadowski, MDPI Energies 2022)

The expansion valve was modelled as an adiabatic throttling process, in which pressure is reduced without work or heat transfer, such that enthalpy is conserved:

$$h_{out} = h_{in} \qquad (5.11)$$

Solution and extraction of results

The system of equations formed by the above equations, together with the specified boundary conditions, were solved iteratively until convergence. Once solved, the condenser duty was extracted directly from the energy balance across the condenser, and is consistent with the first law applied to the cycle as a whole:

$$\dot{Q}_{cond} = \dot{Q}_{evap} + \dot{W}_{comp} \qquad (5.12)$$

expressing that the heat delivered to the district heating network equals the sum of the waste heat absorbed and the electrical work supplied to the compressor.

The coefficient of performance, representing the ratio of useful heat delivered to electrical work consumed, follows as

$$COP = \frac{\dot{Q}_{cond}}{\dot{W}_{comp}} \qquad (5.13)$$

Design basis and capital cost

The heat pump was sized at the 95th percentile of the coldest ambient conditions observed over the year, rather than at the single absolute minimum, in order to avoid oversizing the equipment for a handful of extreme outlier hours. At this design point the district heating return temperature is close to its seasonal maximum, giving the greatest temperature lift across the compressor and therefore the most demanding operating condition the system to have. The coefficient of performance is close to its minimum and the compressor power close to its maximum. The capital cost of the heat pump was estimated on the basis of its rated thermal output,

$$C_{HP} = \dot{Q}_{cond} \cdot c_{HP} \qquad (5.14)$$

where $c_{HP}$is the CAPEX per unit of thermal capacity which is 12,000 SEK/kW_{th} as derived from Danish Energy Agency (2026).

5.4.2 Heat exchanger sizing

The heat exchanger is sized using the logarithmic mean temperature difference (LMTD) method for counterflow geometry, following Incropera et al. (2007) and Shah and Sekulić (2003). The hot side is the source stream and the cold side is the network water stream that is being heated. The four boundary temperatures of the exchanger are denoted T_H,in, T_H,out, T_C,in, T_C,out, with the standard counterflow convention that T_H,in pairs with T_C,out and T_H,out pairs with T_C,in. The LMTD is defined as:

$$LMTD = (\Delta T1 - \Delta T2) / ln(\Delta T1 / \Delta T2) \qquad (5.15)$$

where ΔT_1 = T_H,in − T_C,out and ΔT_2 = T_H,out − T_C,in. The required heat transfer area follows from the heat duty Q_cond (for the HP-fed case) or Q_src (for the direct case), divided by the product of the overall heat transfer coefficient U and the LMTD:

$$A_{HX} = Q/(U \times LMTD) \qquad (5.16)$$

Where U is the overall heat transfer coefficient, taken as 3500 W/ m^2K^1 (Engineering Toolbox, 2003) for a liquid–liquid plate type heat exchanger. A 20 % margin is applied to the calculated area to account for fouling, control imperfections, and the difference between design and worst-case operating conditions. The margin is consistent with the recommendation of the TEMA standards and with the

practice of Swedish district heating substation manufacturers. For the single gas-to-liquid exchanger in Case 4, serving the air-cooled compressor aftercooler stream, a U value of 35 W/m²K is applied, taken from the representative overall heat transfer coefficients tabulated by Bergman (2011) for a finned-tube exchanger with water in the tubes and air in cross-flow. The two-order-of-magnitude difference between the liquid–liquid and gas–liquid coefficients is the dominant factor in the exchanger sizing for that stream, despite carrying the smallest duty of any stream in the study, it requires a disproportionately larger transfer area.

Effectiveness and delivered heat

The effectiveness ε of the exchanger characterises the ratio of actual heat transfer to the thermodynamic maximum and is taken as 55% across all three cases, consistent with the Vlcan (2025) study of industrial waste heat utilization where typical efficiency of industrial heat exchanger falls in the range of 50% to 60%. The delivered heat to the network is:

$$Q_dhn = \varepsilon \times Q_source\text{-}side \quad (5.17)$$

For the AstaReal case, an important nuance is that the Vattenfall measured figure of 14,657 MWh/yr is itself the post-HX delivered heat (i.e., already includes the effectiveness reduction), and the effectiveness is not applied again. For the remaining cases, the effectiveness is applied to the source-side heat to obtain the delivered heat.

Approach temperature programme

The approach temperature programme defines the temperature differences at the two ends of the exchanger and is the principal design choice that balances area against thermodynamic loss. Three programmes are used in the present work, depending on the source temperature relative to the network temperatures. For the low and moderate temperature cases (ICA Maxi, AstaReal), a tight range is used with ΔT_1 = 10 K at the hot end and ΔT_2 = 5 K at the cold end, yielding LMTD = 7.21 K. For the high-temperature Metsä Board case, where the source temperature substantially exceeds the network supply temperature, a wider range is used with ΔT_1 = 35 K and ΔT_2 = 20 K, yielding LMTD = 26.80 K. Case 4 applies two programmes simultaneously, since its streams span different temperature ranges. The two water streams use the low-grade programme, ΔT_1 = 10 K and ΔT_2 = 5 K, giving LMTD = 7.21 K, identical to that used for Cases 1 and 2. The supply-side compressor aftercooler stream uses a wider programme determined by its own terminal temperatures, the cold side is network supply water heated from up to 100 °C, and the hot side is cooling air entering at 179 °C and leaving at 115 °C, giving ΔT_1 = 78.9 K, ΔT_2 = 35 K and LMTD = 54.0 K. The wider programme is appropriate for the high-temperature case because it reduces the heat transfer area, the source temperature being far above the minimum required to deliver heat at the network supply temperature. Because the approach temperatures are held fixed by construction in every case, the LMTD is constant throughout the year. Similar to case with heat pumps, the heat exchanger was sized at the 95th percentile of the coldest ambient conditions observed over the year, rather than at the single absolute minimum, in order to avoid oversizing the equipment for a handful of extreme outlier hours.

The capital cost of the heat exchanger was estimated as a linear function of the required heat transfer area,

$$C_{HX} = A_{HX} \cdot c_{HX} \cdot r_{EUR/SEK} \qquad (5.18)$$

where c_{HX} is the specific installed cost per unit area, taken as 550 EURO/m² for a gasketed plate heat exchanger, following cost data reported by Vlcan (2025)

Table 5.1. *Heat exchanger approach programmes and resulting sizing basis by case.*

Parameter	ICA Maxi	AstaReal	Metsä Board	Case 4 : Air stream	Case 4 : Water stream
Warm-end approach ΔT_1	10 K	10 K	35 K	10 K	78.9 K
Cold-end approach ΔT_2	5 K	5 K	20 K	5 K	35 K
LMTD	7.21 K	7.21 K	26.8 K	7.21 K	54 K
U (W/m²K)	3,500	3,500	3,500	3,500	35
Area margin	20 %	20 %	20 %	20 %	20 %

5.4.3 Pipe network optimisation

Pipe diameter was determined consistently across the three cases through evaluation of the standard EN 253 pre-insulated pipe sizes, from DN 25 up to DN 600, against an infrastructure-level cost objective subject to a velocity constraint of 0.5 to 1.5 m/s. Following the cost-minimisation framework of Frederiksen and Werner (2013), this objective minimises the sum total of pipe capital expenditure, pump operating expenditure, and the economic cost of heat lost through the pipe insulation. As the candidate set comprises only a single connection pipe of standard discrete sizes (DN 20, DN 25, DN 32, DN 50, DN 80, DN 100, DN 150, DN 200, DN 300, DN 400, DN 500, DN 600), this exhaustive search is sufficient to identify the global optimum directly, without using a dedicated optimisation solver.

The mass flow needed to deliver a given duty at a specified injection temperature difference follows from the sensible heat equation:

$$\dot{m} = Q / (Cp\ \Delta T_{dhn}) \qquad (5.19)$$

and the velocity in a pipe of internal diameter d_i is:

$$v = \dot{m} / (\rho \cdot \pi d_i^2 / 4) \qquad (5.20)$$

where d_i is the internal pipe diameter and ΔT_{dhn} is the temperature difference between the district heating supply and return pipelines. A velocity constraint of $0.5 \leq v \leq 1.5$ m s^{-1} was imposed as per Frederiksen and Werner (2013), consistent with established district heating design practice as the

velocities below this range risk sedimentation and oversized capital investment, while higher velocities produce excessive pressure loss and noise.

In Case 4 the optimisation is performed independently for each of the two connection pipes.

The first pipe carries the combined water loop with lengths of approximately 20 m and 15 m respectively.

Frictional pressure drop is computed from the Darcy–Weisbach equation, with the friction factor obtained from the Colebrook–White correlation solved iteratively in pandapipes.

The Colebrook–White equation, an implicit correlation for the Darcy friction factor in pipe flow, is:

$$\frac{1}{\sqrt{f}} = -2log_{10}\left(\frac{\varepsilon}{3.7\,d_i} + \frac{2.51}{Re\sqrt{f}}\right) \qquad 5.21$$

where f is the friction factor, ε is the pipe's absolute roughness, d_i is the internal diameter, and Re is the Reynolds number; because f appears on both sides, pandapipes solves it iteratively updating the friction factor.

$$\Delta P_{fric} = f\,(\rho\, v^2 / 2d_i) \cdot 2L \qquad (5.22)$$

$$\Delta P_{fit} = k_{fit} * \Delta P_{fric} \qquad (5.23)$$

Where Δp_{fric} is the pressure drop due to pipe friction in the straight pipe sections and ΔP_{fit} is the pressure drop due to friction in the pipe fittings. *L* is the one-way pipe lengthand k_{fit} = 0.25 is the fitting-loss factor relative to the straight sections of the pipe.

The total pump head comprises the frictional and fitting losses of the pipe together with the required differential pressure at the injection point Δp_{dhn}:

$$\Delta p_{pump} = \Delta p_{fric} + \Delta p_{fit} + \Delta p_{dhn} \qquad (5.24)$$

where $\Delta p_{dhn}$is the required differential pressure at the district heating injection node which ranges from 1 bar to 4 bar as suggested by Patrik of Vattenfall and applied across all the cases.

The circulation pump power is related to the volumetric flow and the total pressure rise:

$$\dot{W}_{pump} = \dot{V}\,\Delta p_{pump} / \eta_{pump} \qquad (5.25)$$

Where $\dot{V} = \dot{m}/\rho$ the volumetric flow rate and η_{pump} is the pump efficiency assumed to be 0.65 consistent with typical values reported for small-to-medium centrifugal pumps observed to be within 55–70% (Pumps & Systems, 2020)

Pipe heat loss uses the linear heat-loss-relation:

$$\dot{Q}_{loss} = K_{ins}\, L\, (T_{pipe,mean} - T_{ground}) \qquad (5.26)$$

with K_{ins} = 0.55 W/m·K for new pre-insulated pipes as per Frederiksen and Werner (2013), $T_{pipe,mean}$ the mean of the hot- and cold-side pipe temperatures, and T_{ground} = 6 °C the assumed constant ground temperature and L is the length of the pipe.

The capital cost of the pre-insulated district heating connection pipes were estimated from nPro Technologies (2024). The published cost formulation applies to buried pre-insulated pipe. In Case 4 the connection pipes run entirely within the plant boundary, where routing on existing overhead pipe racks would be practicable and would avoid excavation cost. In the absence of a published cost basis for overhead routing, the buried formulation is retained for this case and is treated as a conservative upper bound on the pipe capital cost. Pipe lengths being minimal in case 4, this assumption will not have any major impact on the economics.

5.5 Thermal energy storage

The required thermal energy storage (TES) capacity for each case was determined from a time-series analysis of the temporal mismatch between the waste heat supply profile and the capacity of the district heating (DH) system to receive the available heat or in other words the heating demand. The storage is therefore sized to buffer periods when the waste heat source can provide more heat than the DH system can receive, and to supply the corresponding deficit when the available waste heat falls below the demand.

In the absence of measured hourly DH load data, the receiving capacity or demand of the DH system was represented using a temperature-dependent profile, reflecting the seasonal variation in heat demand. An ambient-temperature-based heating-degree signal was used to describe this variation:

$$\mathrm{HDD(h)} = \max[\mathrm{T_{base}} - \mathrm{T_{amb}(h)}, 0] \qquad (5.27)$$

where T_{base} is the outdoor temperature below which space heating demand increases, taken as 17 °C, and T_{amb}(h) is the hourly ambient temperature from the measured SMHI record for the relevant location.

District heating demand does not fall to zero in summer, because domestic hot water, commercial and industrial loads, and network base demand persist year-round. A non-zero base component was therefore included, and the heating degree signal normalised by its annual mean to give a dimensionless receiving-capacity shape:

$$\mathrm{F(h)} = \mathrm{f_{base}} + (1 - \mathrm{f_{base}}) \times \mathrm{HDD(h)} \,/\, \mathrm{mean(HDD)} \qquad (5.28)$$

where f_{base} is the assumed fraction of year-round base demand, taken as 0.20.

The seasonal shape was then scaled so that its annual energy equals the annual energy available from the waste heat source:

$$\mathrm{Q_{rec}(h)} = \mathrm{F(h)} \times \Sigma\, \mathrm{Q_{src}(h)} \,/\, \Sigma\, \mathrm{F(h)} \qquad (5.29)$$

This scaling does not imply that the waste heat source supplies the complete district heating network demand. It represents the time-varying share of heat that the district heating system is assumed to receive from the specific waste heat source. Imposing equal annual energy establishes a cyclic annual storage condition, so that the charge and discharge energy balance over the year and the analysis isolates the effect of temporal mismatch between source availability and seasonal heat demand.

For Case 4, the receiving-capacity shape was not constructed from a heating-degree signal, because measured district heating demand data were available directly from the plant. The plant records the total net heat delivered to its own network alongside the cooling tower rejection, and the state-of-charge series for this case is constructed at daily rather than hourly resolution, consistent with the data available as described in Section 5.3.3. The seasonal variation in demand was therefore taken from the measured delivery record rather than inferred from ambient temperature

The remainder of the method, Equations 5.30 to 5.34 below, is applied unchanged.

The hourly thermal imbalance between the source and the receiving capacity was calculated as

$$\Delta E(h) = [Q_{src}(h) - Q_{rec}(h)]\,\Delta t \qquad (5.30)$$

where a positive imbalance represents surplus heat available for charging the store, and a negative imbalance represents a deficit that must be supplied by discharging it. The cumulative state-of-charge trajectory follows as

$$SOC_{raw}(t) = \Sigma\,\Delta E(h),\ h = 1\ldots t \qquad (5.31)$$

The required usable storage capacity corresponds to the full operating range of the cumulative energy balance, rather than to its peak alone:

$$E_{req} = \max[SOC_{raw}(t)] - \min[SOC_{raw}(t)] \qquad (5.32)$$

The state of charge was subsequently shifted by its minimum value for graphical representation, such that $0 \le SOC(t) \le E_{req}$:

$$SOC(t) = SOC_{raw}(t) - \min[SOC_{raw}(t)] \qquad (5.33)$$

The required storage volume was obtained from the sensible heat storage relationship for water:

$$V = E_{req} / (c_{p,vol}\,\Delta T_{TES}) \times SF \qquad (5.34)$$

where $c_{p,vol}$ is the volumetric heat capacity of water, taken as 1.16 kWh/(m³·K), ΔT_{TES} is the usable storage temperature difference, and SF = 1.10 is a 10 % safety factor. The usable temperature swing ΔT_{TES} was derived in each case from the temperatures between which the store actually cycles in that system: the temperature at which the store is charged, and the district heating return temperature to which it discharges.

Four seasonal storage technologies are evaluated against this sizing requirement for cases 2 & 3 as per Danish Energy Agency's Technology Data for Energy Storage, Chapter 140: pit thermal energy storage (PTES), borehole thermal energy storage (BTES), aquifer thermal energy storage (ATES) and tank

thermal energy storage (TTES) (Danish Energy Agency and Energinet, 2018). The basis for evaluation are as follows: the CAPEX involved, the achievable capacity range and charge/discharge temperature and speed of each technology; the recovery efficiency and the geological requirement for each technology assessed against the locations of the waste heat sites involved.

For Case 4 the storage technology was not selected through this comparative evaluation. The plant operator has an existing rock cavern development plan for the site, and the analysis therefore adopts rock cavern storage as given rather than as a conclusion. The capital cost for this case is likewise not taken from a published source. The plant supplied a capital cost per cavern directly, which is treated as confidential and is not reproduced in this report

5.6 Dynamic simulation

For each case, a single hourly calculation function brings together the exchanger area, the heat pump's COP, pipe mass flow, pressure drop, pump power, and pipe heat loss driven by the network temperatures and source conditions at that hour. This function is applied across the 8760 hours of the year using NumPy's vectorised operations, with results collected in a Pandas DataFrame and aggregated to monthly and annual totals. For Case 4 the same function is applied across the 365 daily points of the operating year, and is executed once per stream with the results aggregated across streams at the annual level.

The dynamic treatment captures effects a single design point cannot. The heat pump coefficient of performance varies seasonally with ambient temperature; the pump duty varies with the changing difference between the network and injection temperatures; and the pipe heat loss varies with the mean pipe temperature relative to the constant 6 °C ground. The net heat delivered to the network, which serves as the denominator in the LCOH calculation, is defined consistently as the post exchanger heat available minus the calculated pipe heat loss, summed over the year.

5.7 Economic evaluation

Capital costs for the pipes & , heat exchanger, circulation pump, heat pump and thermal storage are annualised with the standard capital recovery factor at a 5 % discount rate over asset-specific lifetimes of 55 years for the pipe, consistent with its EN 253 design life; 20 years for mechanical equipment; and 40 years for thermal storage, following the Danish Energy Agency's technical lifetime for water-based storage. Operating costs for electricity required to run heat pumps and circulation pumps are summed for 8760 hours of the year. Maintenance is included as an annual charge of 1% of installed capital cost, following the operation and maintenance convention published by nPro Technologies (2024), and is applied consistently across all cases.

The capital recovery factor and the levelised cost are:

$$CRF = r(1 + r)^n / [(1 + r)^n - 1] \quad (5.35)$$

$$LCOH = ((\Sigma CAPEX_i * CRF_i) + \Sigma OPEX_i) / \dot{Q}_{net} \quad (5.36)$$

where r = 0.05 is the discount rate, n the asset lifetime, and $\dot{Q}_{net}$ the net annual heat delivered after the heat exchanger net of pipe heat loses.

The resulting LCOH was compared, in every case, against the marginal production cost of the district heat production. This benchmark was obtained by averaging the published seasonal consumer tariff range and applying a factor of 0.7 to strip out network overhead, taxation and profit embedded in the consumer price, following the system-benefit framework of Energiforsk (2022), which holds that the correct compensation for prosumer heat is the avoided marginal cost of generating it elsewhere in the network.

$$C_{DH,marginal} = [(C_{peak,summer} + C_{peak,winter}) / 2] \times f_{corr} \quad (5.37)$$

where $C_{peak,summer}$ and $C_{peak,winter}$ are the published peak summer and peak winter consumer tariffs [SEK/MWh] for the receiving network, and f_corr = 0.7 is the correction factor applied to remove non-production cost components. The summer and winter consumer prices were obtained from Vattenfall Prisändringsmodell (2024) and Övik Energis prisändringsmodell (2026).

For Case 4 the benchmark was not derived from published tariffs. The plant supplied the marginal production cost for its own network directly on the condition that the data remain confidential..

Alongside the breakeven connection-distance was evaluated for the cases 1 to 3, a systematic sweep of pipe length was run for each case, holding all other parameters at baseline, to find the maximum distance at which the levelised cost would still sit below the applicable benchmark.

5.8 Sensitivity and uncertainty analysis

A tornado sensitivity analysis is run for each case across five to ten input parameters including the pipe capital cost, pipe length, annual waste heat quantity, source temperature where relevant, Euro – SEK exchange rate, electricity price, pump efficiency each varied individually over a defined range while the others were held at baseline. Results are reported as percentage deviation from the baseline levelised cost, which allows the influence of each parameter to be compared across cases despite their differing absolute scales.

To capture the combined effect of simultaneous uncertainty, a Monte Carlo simulation of one thousand scenarios was run for each case. Each uncertain parameter was sampled independently from a uniform distribution spanning the same range used in the tornado analysis, so that the two analyses rest on a single, explicitly stated set of parameter bounds. The resulting distribution of levelised cost outcomes gives the probability of viability relative to the applicable benchmark for each case.

5.9 Plant Efficiency Evaluation

This section applies to Case 4 only. In Cases 1 to 3 the waste heat source lies outside the boundary of any plant whose efficiency is defined, and no equivalent metric exists.

Where the waste heat source and the district heating producer are the same facility, the recovered heat can be expressed not only as a cost but as a change in the plant's own thermal efficiency. This provides a second evaluation metric alongside the levelised cost, and one that speaks directly to the operator's own performance reporting.

The metric is defined at the plant boundary rather than at the boiler island. The denominator is the fuel energy entering the plant, calculated from the waste throughput and its lower heating value. The numerator is the total useful thermal energy leaving the plant to the district heating network, comprising the heat delivered through the existing steam cycle together with the additional heat recovered from the waste heat streams identified in this study. This boundary is adopted because two of the four recovered streams originate in auxiliary equipment, specifically the compressor aftercooler and the chiller condenser, rather than in the boiler itself. Heat recovered from a compressor aftercooler is not attributable to the combustion process and would therefore fall outside a boiler efficiency defined on the steam output. It is nevertheless useful thermal output leaving the plant, and it is delivered without any increase in fuel input. The plant boundary is the smallest boundary that contains both the fuel input and all of the recovered streams, and the metric is accordingly reported throughout as a plant efficiency.

The design efficiency η_o quoted by the plant is taken as the reference point against which the improvement is measured. It represents the plant's useful thermal output per unit of fuel energy before any of the recovery measures examined here are implemented. The recovered streams add useful output at the same boundary without any corresponding increase in fuel input, so the revised efficiency is:

$$\eta_{\mathrm{new}} = \frac{\eta_0 \dot{Q}_{\mathrm{fuel}} + \dot{Q}_{\mathrm{recovered}}}{\dot{Q}_{\mathrm{fuel}}} \qquad (5.38)$$

where η_o is the design efficiency which was provided by the plant, Q̇_fuel the fuel energy input calculated from the waste throughput and its lower heating value, and Q̇_recovered the combined duty of the recovery streams.

6. Results and Discussion

This chapter presents the results produced by applying the methodology of Chapter 5 to the four cases introduced in Chapter 4. Each case is treated in turn: the dynamic simulation, component sizing, pipe diameter optimisation, the levelised cost of heat and its comparison against the host network's marginal production cost, and the sensitivity, Monte Carlo analysis and evaluation of improvement in plant boiler efficiency specifically for case 4.

6.1 Case 1: ICA Maxi, Haninge

6.1.1 Key results & Component sizes

Below table 6.1 summarises the resulting component sizes across the heat pump, heat exchanger, connection pipe and booster pump.

Table 6.1. *Component sizing summary, ICA Maxi.*

Component	Design-point value	Notes
Heat pump (R290)	COP 6.6 (winter) – 8.9 (summer)	Floating condenser control
Condenser duty Q_cond	147.1 kW (design)	Evaporator duty Q_evap constant at 124.4 kW
Compressor power W_comp	22.7 kW (design)	Lower in summer as lift reduces
Heat exchanger area	5.83 m²	LMTD 7.21 K, U = 3,500 W/m²K, ε = 0.55
Connection pipe	DN25, 3,500 m	Design velocity 1.14 m/s
Booster pump	5.87 kW (design)	Total pump ΔP = 60.31 bar

6.1.2 Dynamic simulation and Energy Losses

Simulating the full 8,760-hour year, rather than a single winter design point, changes the picture in two ways. First, the floating condenser control scheme raises the coefficient of performance from 6.6 during peak winter to 8.9 in summer when the required temperature lift is smallest. Second, the average heat loss during the month of January is 12.5% more than that during the month of June. This gap is of significance because the design-point calculation would implicitly assume winter conditions persist all year.

Fig 6.1. *Monthly distribution of energy losses, ICA Maxi.*

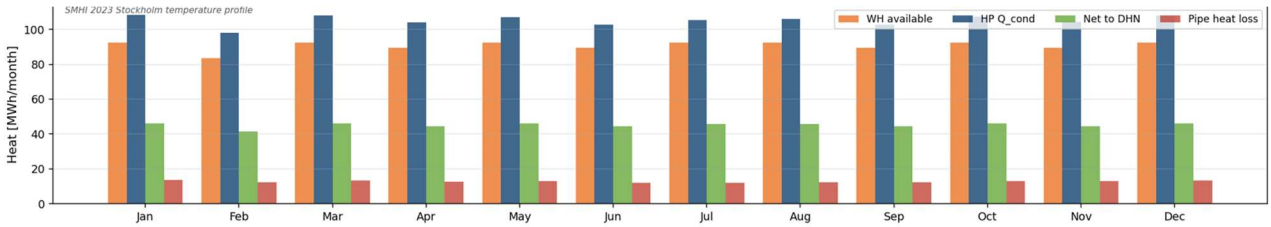

Fig 6.1 shows the hourly simulation results aggregated into monthly totals across the four stages of the ICA Maxi connection. Waste heat available at source stays essentially flat at 89–93 MWh per month, reflecting refrigeration plant that runs independently of season. The heat pump lifts this to 100–108 MWh at the condenser, the small monthly variation arising from the floating condenser

control as the required temperature lift shifts with network return temperature. The heat exchanger effectiveness of 0.55 brings the delivered heat down to 41–46 MWh, and transit losses to ground remove a further 12–16 MWh over the 3,500 m connection. That final loss is the defining feature of this case. It amounts to roughly a quarter of the heat leaving the exchanger. Of the roughly 90 MWh entering the system each month, only about 32 MWh reaches the network. This is not a failure of thermodynamic design but simply the cost of moving a small heat flow a long way.

6.1.3 Pipe Diameter Optimisation

Table 6.2 shows the candidate pipe diameters evaluated for the ICA Maxi connection, with the resulting velocity and associated costs for each. A larger diameter raises pipe CAPEX and heat loss but lowers pump duty through reduced pressure loses due to friction; the optimum balances these effects at the lowest total annualised cost, subject to the 0.5–1.5 m/s velocity constraint from Chapter 5.

Only DN25 and DN32 satisfy this velocity constraint at ICA Maxi's heat duty, and DN25 gives the lower overall cost, so it is selected. This is more evident from the connection distance: at 3,500 m, pipe CAPEX has a dominant influence on the total cost as observed in the below table. So the diameter that minimises pipe cost effectively minimises total cost. The usual benefit of a larger diameter in reducing pumping costs is too small to outweigh the extra capital it demands over such a long run.

Table 6.2. *Pipe diameter optimisation summary, ICA Maxi.*

Pipe	d_i (mm)	d_o (mm)	v (m/s)	Q_{loss} (MWh)	Q_{loss} cost (kSEK)	Pipe CAPEX (kSEK)	Pump OPEX (KSEK)	Total Cost (kSEK)	Vel in range?
DN20	21.6	27	1.725	128.7	539	39271	152.6	39963	FALSE
DN25	**26.6**	**33.4**	**1.138**	**159.2**	**666.8**	**40803**	**56.5**	**41526**	**TRUE**
DN32	**35.4**	**42.2**	**0.642**	**201.2**	**842.4**	**42947**	**17.7**	**43807**	**TRUE**
DN40	41.8	48.6	0.461	231.7	970.2	45398	10.9	46379	FALSE
DN50	54.5	60.3	0.271	287.5	1203.8	48461	7.1	49672	FALSE
DN65	70.3	76.1	0.163	362.8	1519.2	53055	6	54580	FALSE

6.1.4 Levelised cost of heat and economic viability

Fig 6.2. *Cost breakdown and LCOH, ICA Maxi.*

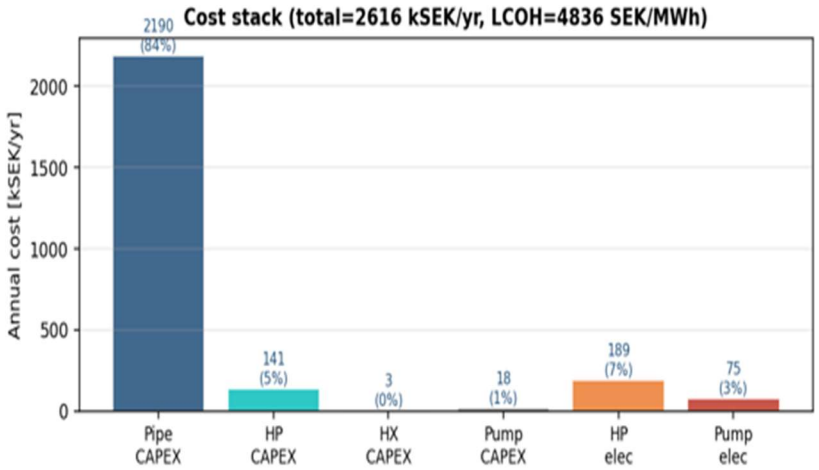

The levelised cost of heat on this basis is 4,836 SEK/MWh, against a marginal production cost benchmark of 347 SEK/MWh for the Vattenfall Stockholm network, a factor of nearly fourteen above the threshold at which the project would be worth pursuing. The dominant cost driver is unambiguous: pipe capital expenditure annuity alone accounts for roughly 82 % of the total annual cost, an order of magnitude larger than any other component. The heat pump, despite requiring the most sophisticated thermodynamic treatment in the methodology, contributes only around 12 % of the total cost and is not the reason the project fails.

A systematic sweep of connection distance places the breakeven point, the distance at which LCOH would equal the 347 SEK/MWh benchmark which is approximately 90 m. Given the actual connection distance of 3,500 m, the ICA Maxi source would need to be roughly forty times closer to the network for this specific project to clear its benchmark on connection cost alone. The verdict is obvious, ICA Maxi, Haninge is not viable at its present location.

6.1.5 Sensitivity and uncertainty

Table 6.3. *Tornado sensitivity ranges tested, ICA Maxi*

Parameter	Range tested
Annual waste heat quantity	±25 %
EUR/SEK exchange rate	9.0–13.5
Pipe lifetime	30–60 yr
Pipe CAPEX	±30 %
Pipe length	±10 %
Electricity price	0.75–1.60 SEK/kWh
Heat pump COP	±20 %
Heat pump CAPEX rate	8,000–16,000 SEK/kW

DHN return temperature	42–52 °C

Fig 6.3. *Tornado sensitivity analysis for LCOH deviation from baseline, ICA Maxi.*

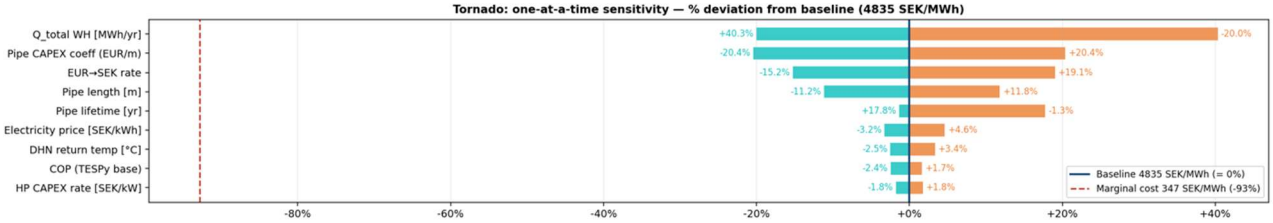

The red dotted line in the above sensitivity analysis chart represents the benchmark which is the levelized cost of district heat production. No single parameter, varied individually across a realistic range, moves the levelised cost anywhere near the marginal cost benchmark, which sits roughly 93 % below the baseline LCOH. This is further confirmed by the Monte Carlo simulation of 1,000 scenarios, which returns a a 5th–95th percentile range of roughly 3,900 to 5,900 SEK/MWh, and a probability of viability of 0.0 %. The conclusion that ICA Maxi is not viable.

Fig 6.4. *Monte Carlo simulation across 1000 scenarios, ICA Maxi.*

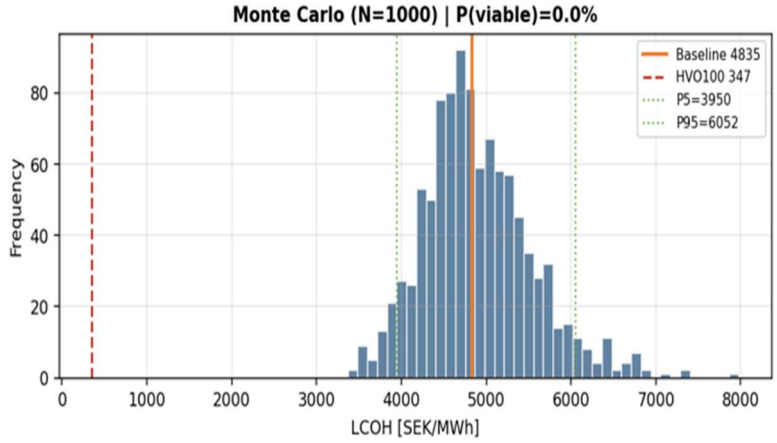

6.1.6 Discussion

The project fails because 1,090 MWh/yr of source heat cannot support a 3,500 m connection. The pipe CAPEX dominates the total annual cost stack at 84%. The low heat quantity coupled with the long connection distance results in 27% of the heat post heat exchange being lost in the connection pipe before reaching the DHN. The ICA Maxi case also demonstrates that thermodynamic sophistication cannot compensate for a large connection infrastructure; modelling the heat pump cycle capturing the seasonal improvement in COP is methodologically important but it is almost irrelevant to the outcome in this case due to the long connection infrastructure.

6.2 Case 2: AstaReal, Gustavsberg

6.2.1 Component sizing

The analysis here begins at the heat exchanger connecting the waste heat from the air conditioner condenser upto to the delivery to the SamEnergi network. We have a seasonal TES considered in this case since the source here has seasonal variations and seasonal shutdowns involved. Below table 6.4 summarises the resulting component sizes.

Table 6.4. *Component sizing summary, AstaReal.*

Component	Design-point value	Notes
Heat exchanger area	115.93 m²	TESPy peak winter; ΔT_warm 10 K / ΔT_cold 5 K; LMTD 7.21 K; 20 % margin
Circulation pump	34.98 kW	Total Head 52 m
Connection pipe	DN150, 160 m	Average velocity = 1.34 m/s
Seasonal TES – PTES storage	128,775 m³	ΔT 25 K

6.2.2 Dynamic simulation and Heat Loses

The dynamic simulation uses real Vattenfall measured hourly delivery data for the 2025 operating year rather than a synthetic profile, so the source-side variability reflects the actual behaviour of the AstaReal process, including the planned shutdown during September and December months. The net annual heat delivered to the network is 14,630 MWh/yr against a measured source heat of 14,657 MWh/yr, with the difference accounted for by pipe heat loss over the short 160 m connection. Mean delivery power across the year is 1,673 kW.

Fig 6.5. *Monthly distribution of energy losses, Asta Real.*

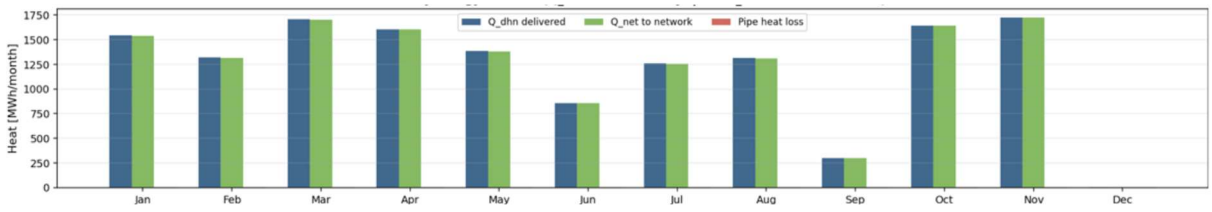

Fig 6.5 shows the hourly simulation results aggregated into monthly totals showing the heat available post the heat exchanger and the heat losses in the connection pipes. By virtue of the high source heat available and low connection distance, the lost heat in the connection pipe is negligible at just 0.18% of the source heat. Hence the red plot representing the pipe heat loss is too small to be visible in the above chart.

6.2.3 Pipe Diameter Optimisation

Table 6.5. *Pipe diameter optimisation summary, Asta Real*

Pipe	d_i (mm)	d_o (mm)	v (m/s)	Q_{loss} (MWh)	Q_{loss} cost (kSEK)	Pipe CAPEX (kSEK)	Pump OPEX (KSEK)	Total Cost (kSEK)	Vel in range?
DN20	21.6	27	73.97	11.3	0.2	1795	478577.4	480372.6	FALSE
DN25	26.6	33.4	48.77	11.3	0.2	1865	160171.5	162036.7	FALSE
DN32	35.4	42.2	27.54	13.9	0.2	1963	35780.2	37743.4	FALSE
DN40	41.8	48.6	19.75	13.9	0.2	2075	14998.7	17073.9	FALSE
DN50	54.5	60.3	11.62	15.7	0.2	2215	3757.5	5972.7	FALSE
DN65	70.3	76.1	6.983	17.6	0.3	2425	1000.8	3426.1	FALSE
DN80	82.5	160	5.07	20.2	0.3	2635	437.1	3072.4	FALSE
DN100	107.1	200	3.009	25.2	0.4	2915	114	3029.4	FALSE
DN125	132.5	225	1.966	28.3	0.4	3266	38.4	3304.8	FALSE
DN150	**160.3**	**250**	**1.343**	**31.5**	**0.5**	**3616**	**14.6**	**3631.1**	**TRUE**
DN200	**210.1**	**315**	**0.782**	**39.7**	**0.6**	**4316**	**3.7**	**4320.3**	**TRUE**

Table 6.5 shows the candidate pipe diameters evaluated for the AstaReal connection, with the resulting velocity and associated costs for each. A larger diameter raises pipe CAPEX and heat loss but lowers pump duty through reduced pressure losses due to friction; the optimum balances these effects at the lowest total annualised cost, subject to the 0.5–1.5 m/s velocity constraint from Chapter 5.

Only DN150 and DN200 satisfy the velocity constraint at AstaReal's heat duty, and DN150 returns the lower cost compared to DN200 pipe as evident in the table. DN150 is therefore selected, which also matches the pipe already installed at the site. The short 160 m connection means the heat loss does not really influence the total cost.

6.2.4 Thermal energy storage sizing and technology selection

The AstaReal source delivery is not continuous and there are planned maintenance with seasonal shutdown, so thermal storage is required to buffer the mismatch. Applying the state-of-charge method described in Chapter 5 against a variable heat demand gives a seasonal storage requirement of 128,775 m^3 once the 10 % safety factor is applied.

Technology screening

Four seasonal storage concepts covered by the Danish Energy Agency's Technology Data for Energy Storage, Chapter 140 were evaluated: pit thermal energy storage (PTES), borehole thermal energy storage (BTES), aquifer thermal energy storage (ATES) and tank thermal energy storage (TTES) (Danish Energy Agency and Energinet, 2018). Screening the AstaReal requirement against the operating

requirements eliminates three of the four before any cost comparison is required. Afterall DEA states that PTES is the most cost-effective solution for large storage volumes.

Aquifer storage is excluded on temperature grounds. The catalogue describes ATES explicitly as a low temperature heat storage technology, with a maximum average storage temperature of 20 °C and a peak of 25 °C under Danish law, against a natural groundwater temperature of 8.5–11 °C (Danish Energy Agency and Energinet, 2018). The AstaReal source arrives at 70–75 °C and must be returned to the network at supply temperature; storing it in a 20 °C medium would require an intermediate heat pump on both charge and discharge, adding cost and complexity. DEA further records that high-temperature ATES requires more research to ensure reliable operation, placing it outside the range of proven application. The technology's recovery efficiency, at 40–80%, is also the widest and least predictable of the four options, reflecting its sensitivity to aquifer permeability and natural groundwater flow (Baeuerle, 2025).

Borehole storage (BTES) is excluded on maturity and operating reasons. DEA states that a typical BTES operates at low temperatures, 0 to 30 °C, and, while acknowledging that operation up to 90 °C is possible, records only a single pilot installation of that type, at Brædstrup. The three reference installations tabulated in the catalogue: Drake Landing, Crailsheim and Brædstrup have storage capacities of 700, 1,135 and 400 MWh respectively, all below the AstaReal requirement, and DEA lists full-scale demonstration as an outstanding research objective rather than a proven capability. (Danish Energy Agency and Energinet, 2018) Three operational disadvantages identified in the catalogue goes against selecting this technology: a buffer tank is required, a heat pump is required, and charging and discharging are slow. The last is decisive here, since the store must absorb a continuously delivered industrial output. Recovery efficiency, at 70–80%, is also structurally lower than PTES because thermal insulation can only be installed at the surface of a BTES field, heat is lost through the sides and base of the storage volume throughout the cycle rather than only at a single insulated boundary (Baeuerle, 2025).

Tank storage is excluded on scale. DEA notes that the largest such installation, in Germany, is 12,000 m^3 (Danish Energy Agency and Energinet, 2018), roughly one eleventh of the AstaReal requirement. The underlying reason is structural, a TTES tank, whether above or below ground, is an engineered steel or concrete vessel that must independently bear the full weight and pressure of the stored water column, whereas PTES, BTES and ATES all use the surrounding soil, rock, or aquifer to provide this structural support at negligible additional cost. The enclosure structure is consequently the dominant cost driver for TTES, rather than the storage medium itself, and this cost does not benefit from the same economy of scale that soil or rock excavation exhibits at large volume (Baeuerle, 2025).

Pit thermal energy storage satisfies the envelope. The catalogue describes PTES as developed for operation at relatively high temperature levels, up to 90 °C all year round, increasing the area of application to excess heat from industries and waste incineration, which is precisely the application examined here. DEA gives typical PTES volumes as 50,000–500,000 m^3, within which the AstaReal

requirement falls, and states directly that PTES is the most commonly used large thermal storage technology in Denmark and initial demonstrations showed that this is the most cost-effective solution for large volumes. (Danish Energy Agency and Energinet, 2018). PTES also achieves the highest recovery efficiency of the four DEA-screened technologies, at 90–95%, a consequence of the strong thermal stratification achievable in a water-filled pit with a floating insulated lid. (Baeuerle, 2025)

Table 6.6. *Seasonal storage technology screening against DEA Chapter 140 operating envelopes, AstaReal.*

Criterion (DEA Ch. 140)	PTES	BTES	ATES	TTES
Max. storage temperature	90 °C year-round	0–30 °C; 90 °C pilot only	20 °C (25 °C peak)	High
Charge/discharge speed	Quick, high capacity	Slow	Fast, but low ΔT	Quick
Heat pump required?	No	Yes	Yes	No
Buffer tank required?	No	Yes	No	No
Largest reference installation	210,000 m³ (Vojens)	37,500 m³ soil (Crailsheim)	1.5 MW (Bjerringbro)	12,000 m³ (Germany)
Reference capacity range	up to 12,180 MWh	400–1,135 MWh	—	—
Recovery efficiency	90 – 95%	70 – 80%	40 – 80%	
Suitable for AstaReal?	Yes	No	No	No

Physical dimensioning

PTES was therefore selected. Applying DEA's dimensioning relationships for a square-footprint pit,

$$d = 0.382 \times V^{0.33}$$

$$A = 20.15 \times V^{0.61}$$

together with the catalogue's stipulated 10 % additional area allowance for rainwater management, materials handling and ancillary activities, gives a water depth of 19.3 m and a footprint of 26,380 m², rising to 29,018 m² with the allowance included. (Danish Energy Agency and Energinet, 2018)

Capital cost

Capital cost follows DEA's 2024 budget-price relationship for PTES,

$$\text{CAPEX (M€)} = 1.84 + 42.00 \times 10^{-6} \times V$$

derived from realised Danish project costs with V being the storage volume in cubic meter (Danish Energy Agency and Energinet, 2018)

Table 6.7. *Seasonal PTES cost summary, AstaReal.*

Parameter	Value
Water volume	128,775 m³
Water depth / footprint	19.3 m / 29,018 m²
PTES CAPEX	7.25 M€ (79.7 MSEK)
Annualised CAPEX (5 %, 40 yr)	4,647 kSEK/yr
Fixed O&M (DEA, 101.2 SEK/MWh)	344 kSEK/yr
Total annualised cost	4,990 kSEK/yr

6.2.5 Levelised cost of heat and economic viability

Fig 6.6. *Cost breakdown and LCOH, AstaReal.*

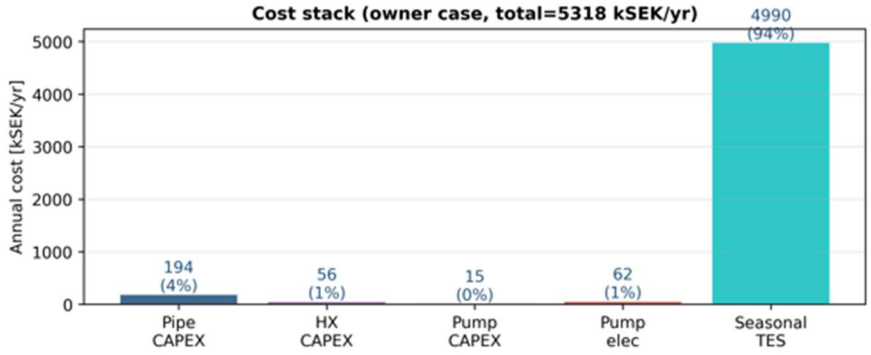

Seasonal storage is the largest single item at 94% of the total, followed by Pipe CAPEX at 4%. As opposed to the ICA Maxi case, the comparatively modest pipe share reflects the short connection distance at 160 m the pipe is simply not expensive enough to govern the outcome, which turns out as the key economic enabler for this case.

The levelised cost of heat in this case is 364 SEK/MWh against a marginal production cost benchmark of 347 SEK/MWh for the SamEnergi network. LCOH clearly exceeds the marginal production cost. Total annualised cost across all components is 5318 kSEK/yr against 14,630 MWh/yr of delivered heat.

6.2.6 Sensitivity and uncertainty

Table 6.8. *Tornado sensitivity ranges tested, AstaReal.*

Parameter	Range tested
Pump efficiency	±10 %
Annual waste heat quantity	±15 %
EUR/SEK exchange rate	±15 %
Electricity price	±15 %

Pipe CAPEX coefficient	±15 %
PTES CAPEX	±10 %

Fig 6.7. *Tornado sensitivity analysis for LCOH deviation from baseline, AstaReal.*

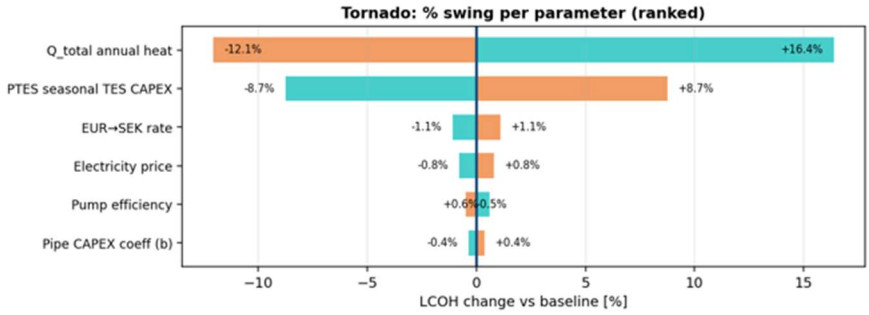

Annual waste heat quantity is the dominant sensitivity in this case, producing a swing of −12.1 % to +16.4 % in levelised cost followed by PTES CAPEX producing a swing of +/- 8.7%. Remaining uncertainties contribute to less than ±1.2 % each.

Fig 6.8. *Monte Carlo simulation across 1000 scenarios, AstaReal.*

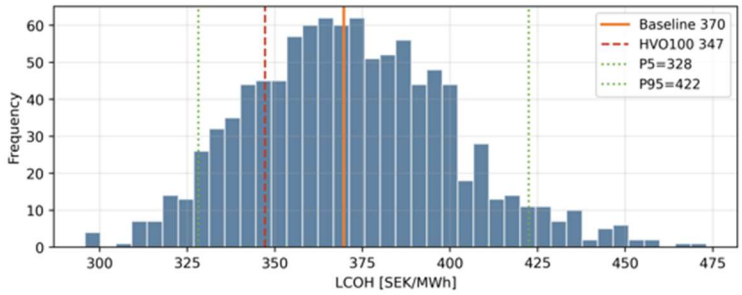

The red dotted line above represents the benchmark for this case. The Monte Carlo simulation of 1,000 scenarios returns a probability of viability of 27.6 % tipping the project towards non-viability

6.2.7 Discussion

AstaReal has almost everything in its favour. The connection is short at 160 m, the source arrives already at network-grade temperature so no heat pump is needed within the thesis boundary, and pipe heat loss is negligible. Excluding seasonal storage, the levelised cost is just 22 SEK/MWh, around a sixteenth of the benchmark.

It still fails. With the store included, the levelised cost rises to 364 SEK/MWh against a 347 SEK/MWh benchmark, and the Monte Carlo returns only a 27.6% probability of viability. The cost stack shows why: the 128,775 m³ store accounts for 94% of annual cost, at 4,990 kSEK/yr against 328 kSEK/yr for the pipe, heat exchanger and pump combined.

The real question is therefore not whether the connection is worth building, but whether 128,775 m³ of storage, occupying 29,018 m² at nearly 20 m depth, is worth building to capture a 14.7 GWh/yr source. Against the SamEnergi marginal production cost, the answer is no.

Two things could tip the case back. First, cavern storage may be a game changer here, though the saving comes from reusing an existing cavity rather than excavating a new one, since CTES is otherwise a high-cost technology (Baeuerle, 2025). Sweden has precedent at Avesta and the 300,000 m³ Västerås site, and engineers there report that "there are a lot of empty, disused underground bunkers that could be converted to thermal energy storage," with "plans already being made in several other locations, including Gävle and Sundsvall" (Winkler, cited in FVB, 2025). Whether such a cavity exists near Gustavsberg is not established here, as no public register documents decommissioned caverns. Second, and more directly, the seasonal mismatch need not be absorbed at this node at all. If Vattenfall's other generation assets take it up, no dedicated store is needed and the connection reverts to 22 SEK/MWh, clearing the benchmark comfortably. That is the more likely route to a viable AstaReal connection.

6.3 Case 3: Metsä Board, Husum

6.3.1 Component sizing

The analysis begins at the heat exchanger connecting the mill's process waste heat to the Övik Energi network. No heat pump is required, since the source temperature of approximately 150 °C exceeds the network's requirement and the exchanger injects directly into the DHN supply main. A seasonal TES is considered in this case since the source here is not continuous and has annual maintenance periods with seasonal shutdown. Below Table 6.9 summarises the resulting component sizes.

Table 6.9. *Component sizing summary, Metsä Board.*

Component	Design-point value	Notes
Heat exchanger area	468 m²	TESPy peak; ΔT_warm 35 K / ΔT_cold 20 K; LMTD 26.80 K at design; 20 % margin
Circulation pump	192.2 kW	Total head 52 m
Connection pipe	DN500, 900 m	Average velocity = 0.988 m/s
Seasonal TES – PTES storage	531,459 m³	

6.3.2 Dynamic simulation and heat losses

The source profile is derived from real hourly steam production data at an anonymised comparable board mill for the 2024 calendar year, thermodynamically converted to a heat delivery profile and rescaled to the confirmed 179,000 MWh/yr annual total for Husum. The profile has a mean delivery of 20.43 MW, interrupted by an October maintenance period and a December month shutdown. The net annual heat delivered to the network is 98,045 MWh/yr, obtained by applying the 0.55 exchanger effectiveness to the source-side total and subtracting pipe heat loss over the 900 m connection, equivalent to hardly 0.2 % of the source heat. The heat loss being negligible in comparison with the source heat, it is invisible in the below chart.

Fig 6.9. *Monthly distribution of energy losses, Metsä Board*

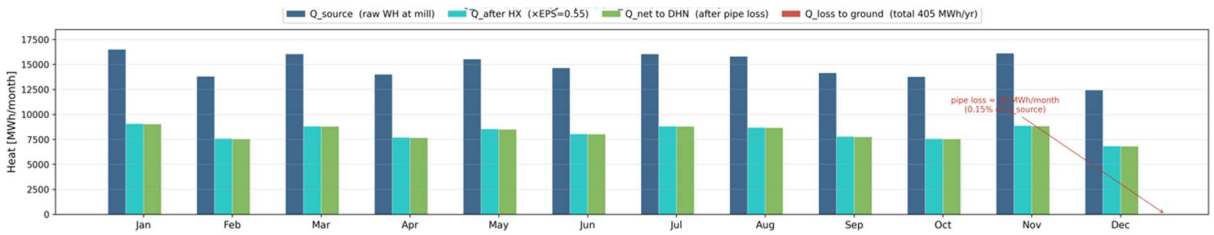

6.3.3 Pipe Diameter Optimisation

Table 6.10. *Pipe diameter optimisation summary, Metsä Board.*

Pipe	d_i (mm)	v (m/s)	Q_{loss} (MWh)	Q_{loss} cost (kSEK)	Pipe CAPEX (kSEK)	Pump OPEX (KSEK)	Total Cost (kSEK)	Vel in range?
DN150	160.3	10.02	112.77	1.71	20337.61	26259.69	46599.03	FALSE
DN200	214	5.62	142.09	2.16	24275.79	5881.11	30159.07	FALSE
DN250	262.7	3.73	160.14	2.43	28213.96	2042.01	30258.41	FALSE
DN300	312.7	2.63	191.71	2.91	32152.13	833.87	32988.92	FALSE
DN400	406.9	1.55	252.61	3.84	40028.47	216.91	40249.23	FALSE
DN500	**510.6**	**0.98**	**311.26**	**4.74**	**47904.81**	**68.48**	**47978.04**	**TRUE**
DN600	**610.1**	**0.69**	**372.15**	**5.66**	**55781.15**	**27.89**	**55814.71**	**TRUE**

A larger diameter raises pipe CAPEX and heat loss but lowers pump duty through reduced pressure loses due to friction. The optimum balances these effects at the lowest total annualised cost, subject to the 0.5–1.5 m/s velocity constraint from Chapter 5. Table 6.10 shows the candidate pipe diameters evaluated for the Metsä Board connection, extended to DN500 and DN600 to reflect the much larger mass flow associated with a 20.43 MW mean delivery. Only these two diameters satisfy the 0.5–1.5 m/s velocity constraint and every smaller diameter is infeasible on velocity alone, well before cost is considered. DN500 returns the lower cost among the two and is therefore selected.

6.3.4 Thermal energy storage sizing and technology selection

Applying the state-of-charge method described in Chapter 5 against a constant reference source rate gives a seasonal storage requirement of 531,459 m³ once the 10 % safety factor is applied.

Technology screening

The same four seasonal storage concepts were evaluated against the Metsä Board requirement using the DEA Chapter 140 operating envelopes (Danish Energy Agency and Energinet, 2018). Aquifer storage is again excluded on temperature grounds as the source is entirely incompatible with ATES's 20 °C ceiling, and at 20.43 MW mean delivery this case exceeds DEA's stated ATES application range of 500 kW–5,000 kW by more than a factor of four. ATES's recovery efficiency of 40–80% is, in any case, the least predictable of the screened technologies, and this uncertainty is compounded here by the much larger scale of the requirement. Borehole storage is excluded for the same operating reasons as

AstaReal, all three DEA reference installations fall far below the Metsä Board requirement, and the slow charge/discharge characteristic of BTES is a still greater mismatch here given the mill's continuous delivery. Tank storage is excluded on the same structural grounds as AstaReal, made more acute by scale. The largest installation in the DEA catalogue, at 12,000 m³, is under three per cent of the Metsä Board requirement, and a TTES facility large enough to hold even a fraction of this volume would need an engineered vessel bearing the full weight of that water column independently, with no natural ground or rock support. The cost of the enclosure structure itself, which dominates TTES economics at any scale, would be expected to scale far less favourably than the excavation-based cost of PTES at this size (Baeuerle, 2025)

Pit thermal energy storage again satisfies most of the requirements and is the only technology of the four able to hold a store of this scale with the highest recovery efficiency of the four screened technologies at 90–95%.

Cavern thermal energy storage is a more interesting supplementary consideration for Metsä Board, given the much larger scale involved. Finland's planned 1,000,000 m³ CTES facility at Vantaa, operating at 140°C for district heating and due to begin operation in 2026, demonstrates that a purpose-built cavern at a scale exceeding even the Metsä Board requirement is achievable (Baeuerle, 2025). CTES is characterised in the literature as high capital cost as a category, and the saving relative to PTES depends specifically on reusing an existing decommissioned cavity rather than mining a new one (Baeuerle, 2025). Sweden has an own example at comparable scale, the 300,000 m³ Västerås facility, converted from a decommissioned oil storage cavern is a reused cavity rather than a purpose built one, and no such cavity has been identified near Örnsköldsvik from literature or public data. CTES is accordingly noted here as worth a dedicated feasibility study rather than as a costed alternative.

Table 6.11. *Seasonal storage technology screening against DEA Chapter 140 operating envelopes, Metsä Board.*

Criterion (DEA Ch. 140)	PTES	BTES	ATES	TTES
Max. storage temperature	90 °C year-round	0–30 °C; 90 °C pilot only	20 °C (25 °C peak)	High
Charge/discharge speed	Quick, high capacity	Slow	Fast, but low ΔT	Quick
Heat pump required?	No	Yes	Yes	No
Buffer tank required?	No	Yes	No	No
Largest reference installation	210,000 m³ (Vojens)	37,500 m³ soil (Crailsheim)	1.5 MW (Bjerringbro)	12,000 m³ (Germany)
Reference capacity range	up to 12,180 MWh	400–1,135 MWh	—	—
Recovery Efficiency	90 – 95%	70 – 80%	40 – 80%	
Suitable for Metsä Board?	Yes	No	No	No

Physical dimensioning

PTES was therefore selected. Applying DEA's dimensioning relationships for a square-footprint pit,

$$d = 0.382 \times V^{0.33}$$

$$A = 20.15 \times V^{0.61}$$

together with the catalogue's stipulated 10 % additional area allowance, gives a water depth of 30.9 m and a footprint of 62,634 m², rising to 68,898 m² with the allowance included (Danish Energy Agency and Energinet, 2018).

Capital cost

Capital cost follows the same DEA 2024 budget-price relationship used for AstaReal,

$$\text{CAPEX [M€]} = 1.84 + 42.00 \times 10^{-6} \times V$$

Table 6.12. *Seasonal PTES cost summary, Metsä Board.*

Parameter	Value
Water volume	531,459 m³
Water depth / footprint	30.9 m / 68,898 m²
PTES CAPEX	24.16 M€ (265.8 MSEK)
Annualised CAPEX + O&M (5 %, 40 yr)	19,175 kSEK/yr

At 531,459 m³ the storage is roughly 2.5 times the largest PTES installation actually built in Denmark (Vojens, 210,000 m³).

6.3.5 Levelised cost of heat and economic viability

Fig 6.9. *Cost breakdown and LCOH, Metsä Board.*

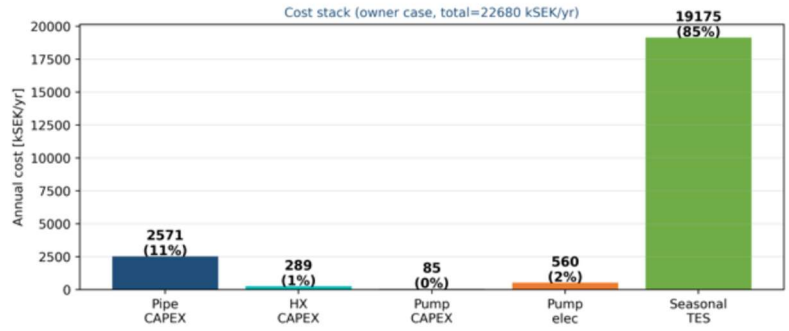

Seasonal storage dominates the cost stack at 85 % of the total annual cost, followed by pipe CAPEX at 11 %. The heat exchanger, pump capital and pump electricity together account for the remaining 4 %.

The levelised cost of heat is 231 SEK/MWh against a marginal production cost benchmark of 263.2 SEK/MWh for the Övik Energi network. A systematic sweep of connection distance places the breakeven point at 1945 m, against an actual connection distance of 900 m giving a comfortable headroom of about 1 kilometer.

6.3.6 Sensitivity and uncertainty

Table 6.13. *Tornado sensitivity ranges tested, Metsä Board.*

Parameter	Range tested
Q_total waste heat	±15 %
Seasonal TES cost	±15 %
EUR/SEK exchange rate	±15 %
Pipe length	±15 %
Electricity price	±15 %
Pipe CAPEX coefficient	±15 %
WH source temperature	±15 %

Fig 6.10. *Tornado sensitivity analysis for viability-ratio deviation from baseline, Metsä Board.*

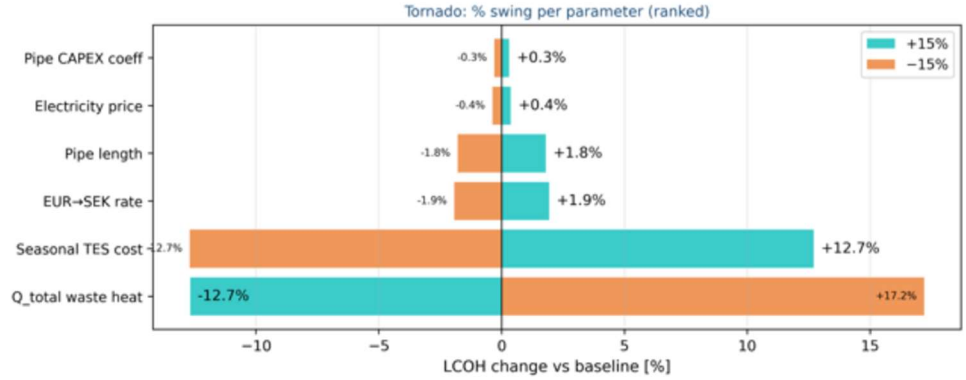

Annual waste heat is the dominant sensitivity in this case, producing a swing of +17.2 % to −12.7 % in the viability ratio, larger than any cost-side parameter. Seasonal PTES cost follows closely at ±12.7 %. EUR/SEK rate, pipe length, electricity price and pipe CAPEX each contribute 2 % or less variation.

Fig 6.11. *Monte Carlo simulation across 1000 scenarios, Metsä Board.*

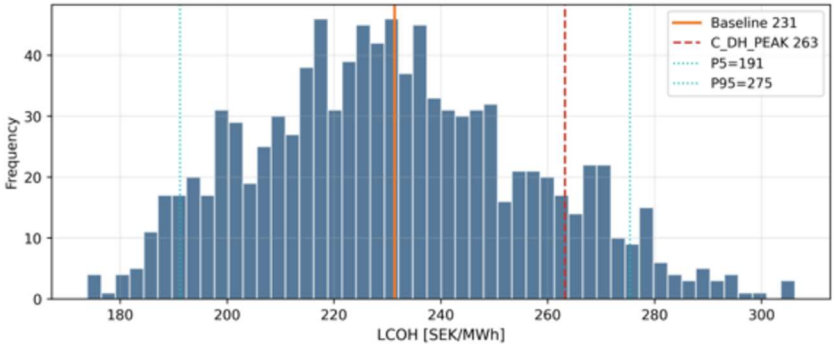

The Monte Carlo simulation returns a probability of viability of 86.4 % against the fixed benchmark making the project a highly viable one.

6.3.7 Discussion

Metsä Board resembles AstaReal. Both carry a seasonal store that dominates their cost stack, but here the store is affordable while at AstaReal it was not. The levelised cost of 231 SEK/MWh against a benchmark of 263 SEK/MWh gives a safe margin, and the Monte Carlo returns an 86.4% probability of viability.

The difference is scale on the delivery side rather than restraint on the storage side. The store is far larger in absolute terms, at 531,459 m³ against AstaReal's 128,775 m³. But it is spread across 98 GWh/yr of delivered heat rather than 14.7 GWh/yr. The higher source temperature also helps materially. Because the heat exchanger boosts the district heating supply to 115 °C and the store discharges to a 50 °C return, the swing is 65 K against AstaReal's 25 K. Each cubic metre therefore holds more than twice the energy, which is why a storage requirement 11 times larger in energy terms translates to a store only 4 times larger in volume.

The breakeven sweep shows where the remaining margin sits. The breakeven distance is 1,945 m against an actual 900 m connection, giving roughly 1,045 m of headroom, around 2.2 times the distance actually required. Read together with AstaReal and ICA Maxi, the three cases sharpen the rule of thumb. Proximity to the network matters, but delivered volume is also crucial to determine whether a seasonal store can be afforded at all.

Two considerations could widen that margin further. First, cavern thermal energy storage is a more interesting prospect here than at AstaReal given the scale involved, and Finland's planned 1,000,000 m³ CTES at Vantaa demonstrates that a purpose-built cavern at this scale is achievable. The real saving over PTES comes from reusing an existing cavity rather than excavating a new one, as at Sweden's Avesta and 300,000 m³ Västerås sites, since CTES is otherwise a high-cost technology (Baeuerle, 2025). Whether such a cavity exists near Örnsköldsvik is not established by this thesis, as no public register documents decommissioned caverns. The prospect is not unreasonable, however: engineers involved in the Västerås conversion report that "there are a lot of empty, disused underground bunkers that could be converted to thermal energy storage," adding that "plans are already being made in several other locations, including Gävle and Sundsvall" (Winkler, cited in FVB, 2025), the latter considerably closer to Örnsköldsvik. Second, if Övik Energi's other generation assets absorb the seasonal mismatch, no dedicated store is required at this node and the levelised cost falls to 36 SEK/MWh, a seventh of the benchmark.

6.4 Case 4: Waste to Energy CHP Plant

Note on reporting convention: at the plant's request the marginal production cost benchmark and the rock cavern capital cost are not reproduced numerically in this report. Where a result would allow either figure to be recovered by back-calculation, it is expressed instead as a viability ratio R, defined as the levelised cost of heat divided by the marginal production cost of the host network, such that R < 1 indicates a viable project. This is the same normalisation applied to the tornado analysis in Section 7.3.6. The cavern capital figure supplied by the plant is a total budget for the storage scheme and is inclusive of operation and maintenance costs.

6.4.1 Component sizing

The analysis begins at the three heat exchangers connecting the plant's continuous auxiliary waste heat streams to the connection pipes. No heat pump is required in this case since the blended water-based streams and the compressor aftercooler air stream both clear their respective injection temperature thresholds by direct exchange. Seasonal storage for heat rejection from cooling towers is treated separately.

Applying the stream-combination logic of Section 6.3.4, the soot blower drain at 58 °C and the chiller condenser at 42 °C are combined into a single recovered-water loop. The heat-weighted average of the two, at 640 kW combined, is 50.7 °C which comfortably sits above the mean network return temperature. The chiller condenser at 42 °C could not have been injected in isolation, it becomes usable only because the warmer soot blower stream lifts the blend above the return threshold. The compressor aftercooler air stream is kept on a separate circuit and injected on the supply side.

Table 6.14. *Component sizing summary, Case 4.*

Component	Design-point value	Notes
Heat exchanger, HS-4 soot drain	16.6 m²	ΔT_1 10 K / ΔT_2 5 K; LMTD 7.21 K; U = 3,500 W/m²K; 20 % margin
Heat exchanger, HS-9 chiller condenser	13.8 m²	As above
Heat exchanger, HS-8 compressor	11.5 m²	ΔT_1 78.9 K / ΔT_2 35 K; LMTD 54.0 K; U = 35 W/m²K
Total exchanger area	41.9 m²	
Water side connection pipe	DN65, 20 m	Average velocity 1.41 m/s; return-side injection
Compressor air connection pipe	DN15, 15 m	Average velocity 0.66 m/s; supply-side injection
Circulation pumps	0.992 kW	Total head 115 kPa
Seasonal storage	436,321 m³	5 caverns of 95,000 m³ installed

The total exchanger area is 41.9 m². The compressor aftercooler exchanger is nonetheless disproportionate to its duty: at 18 kW it carries under three per cent of the combined continuous heat but requires 27 % of the installed area, a direct consequence of the gas-to-liquid heat transfer coefficient being two orders of magnitude below the liquid-to-liquid value.

6.4.2 Dynamic simulation and heat losses

The simulation is executed on the 365-point daily series described in Section 6.3.3 rather than on an 8,760-hour basis, consistent with the resolution at which the plant records its process data.

Across the operating year the boiler delivers a mean output of 58.6 MW. Cooling-tower rejection is taken directly from the plant's own heat meter on the cooling tower circuit, summed across the operating year to give 23,871 MWh, with a daily-average mean of 3.19 MW and a maximum of 24.9 MW.

Fig 6.12. *Monthly recoverable heat and cooling-tower rejection, Case 4.*

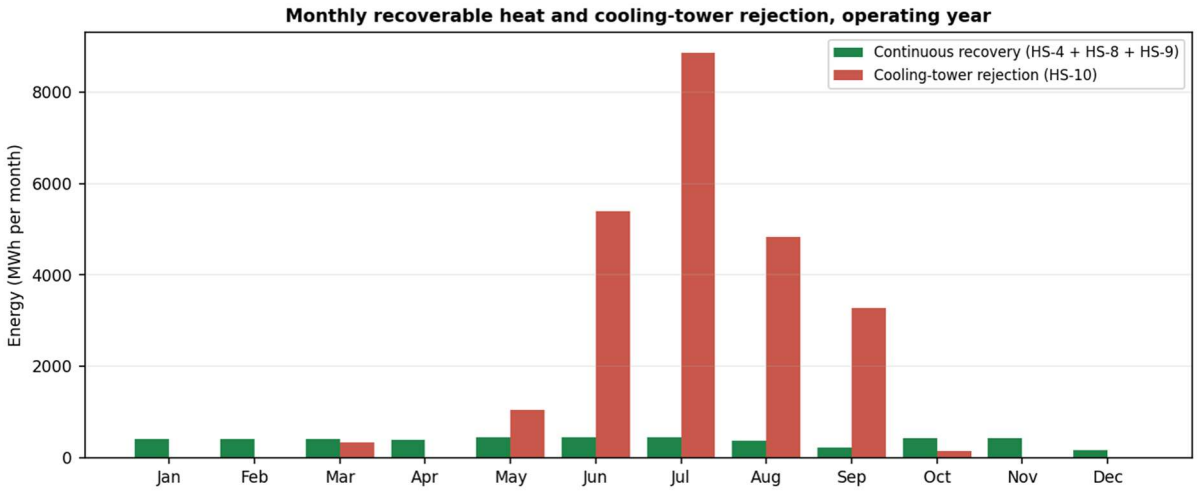

Fig 6.12 shows the daily simulation results aggregated into monthly totals. The three continuous streams deliver a nearly flat 380–490 MWh per month represented by green plot, governed by auxiliary systems that run independently of season. Cooling-tower rejection represented by red plot behaves in the opposite different, it is essentially zero from November through April, rises through May, and peaks at 8,864 MWh in July. Of the 23,871 MWh rejected across the year, 23,406 MWh, or 98 %, falls in the five months from May to September.

Pipe heat loss is negligible in this case and is not shown separately. Over combined connection lengths of 35 m the calculated annual loss amounts to under 0.1 % of the heat delivered. The net heat delivered to the network from the continuous streams is therefore 4,540 MWh/yr, essentially equal to the post-exchanger figure.

6.4.3 Pipe diameter optimisation

Two connection pipes carrying waste heat from water and air-based heat streams are optimised independently, since the streams converge on different injection points. Both carry water and the distinction between them lies in the medium of the waste heat source upstream of each exchanger.

Table 6.15. *Pipe diameter optimisation summary, Case 4.*

Pipe	d_i (mm)	v (m/s)	Pipe CAPEX (kSEK)	Δp total (kPa)	Pump (kW)	Total ann. (kSEK/yr)	Vel. in range?
Water loop (HS-4 + HS-9), 20 m, 5.46 l/s							
DN40	41.8	3.98	259	305.3	2.566	35.6	FALSE
DN50	54.5	2.34	277	153.2	1.288	25.7	FALSE
DN65	**70.3**	**1.41**	**303**	**114.8**	**0.965**	**24.4**	**TRUE**
DN80	**82.5**	**1.02**	**329**	**106.7**	**0.897**	**25.3**	**TRUE**
DN100	**107.1**	**0.61**	**364**	**101.8**	**0.856**	**26.8**	**TRUE**
DN125	132.5	0.40	408	100.6	0.846	29.1	FALSE
Compressor loop (HS-8), 15 m, 0.154 l/s							
DN15	**17.3**	**0.66**	**162**	**115.8**	**0.027**	**8.9**	**TRUE**
DN20	21.6	0.42	168	105.3	0.025	9.2	FALSE
DN25	26.6	0.28	175	101.9	0.024	9.6	FALSE

Pipe heat loss being negligible here, the pipe diameter optimisation is carried out by minimising the cost from pipe capex and pumping costs with the velocity constraints similar to earlier cases. For the water loop, DN65, DN80 and DN100 satisfy the velocity constraint and DN65 returns the lowest annualised cost. DN65 is therefore selected at 1.41 m/s. For the compressor aftercooler air loop the duty is so small that only DN15 falls within the velocity window, every larger diameter dropping below the 0.5 m/s lower bound. This is the reason the candidate set was extended downward from the DN25 pipe size.

Despite the pipes being overground running within the plant, the buried-pipe cost formulation has been retained from nPro is, as noted in Section 5.4.3. It is a conservative upper bound assumption for connections routed inside the plant. Pipework contributing to under one per cent of the full-system cost stack, the conservative approach does not affect the verdict.

6.4.4 Thermal energy storage sizing

Applying the state-of-charge method of Section 5.5 to the measured cooling-tower rejection profile against the plant's own measured network demand gives a peak-to-trough requirement of 19,739 MWh, which at the derived usable temperature swing of 42.9 K translates to a required volume of 436,321 m³. This was rounded up to five caverns of 95,000 m³ each, the standard individual cavern size identified by the plant, giving an installed volume of 475,000 m³.The storage technology is not selected by comparative screening in this case. As described in Section 5.5, the plant operator has an existing rock cavern development plan, and the analysis adopts cavern storage as given.

Table 6.16. *Seasonal storage configuration, Case 4.*

Parameter	Value
Peak state of charge (E_req)	15,009 MWh
Usable temperature swing ΔT_TES	30 K
Required volume (Eq. 6.28–6.29)	436,321 m³
Caverns required	5 × 95,000 m³

Installed volume	475,000 m³
Annual energy throughput	23,871 MWh/yr
Storage lifetime	40 yr
O&M	Included within operator's total budget

The capital cost was supplied by the operator as a total budget for the cavern scheme and is treated as confidential. One observation can be made without reproducing it. The implied unit cost, is materially lower than the specific cost returned by the Danish Energy Agency pit storage relationship applied to Cases 2 and 3 at comparable volume. Developing the existing rock cavern storage for this project is therefore not more expensive than constructing a new pit storage.

6.4.5 Levelised cost of heat and economic viability

The economic analysis using LCOH will be done in three scenarios; first considering the continuous waste heat streams, second the waste rejection from the cooling tower to cavern seasonal storage and third the combination of the first two.

Continuous recovery

The three continuous streams deliver 4,540 MWh/yr for a total installed capital cost of 724 kSEK, comprising 253 kSEK of heat exchangers, 465 kSEK of connection pipework and 5.5 kSEK of pumps. The total annualised cost is 53.7 kSEK/yr and the resulting levelised cost of heat is 11.8 SEK/MWh, an order of magnitude below the marginal production cost benchmark. R value being under 0.1, the continuous heat stream integration into the network is a highly viable prospect. R is the viability ratio which is ratio of waste heat LCOH to the Marginal cost of heat production.

Fig 6.14. *Cost breakdown, Case 4: continuous recovery cost stack (left) and full-system share of annual cost (right).*

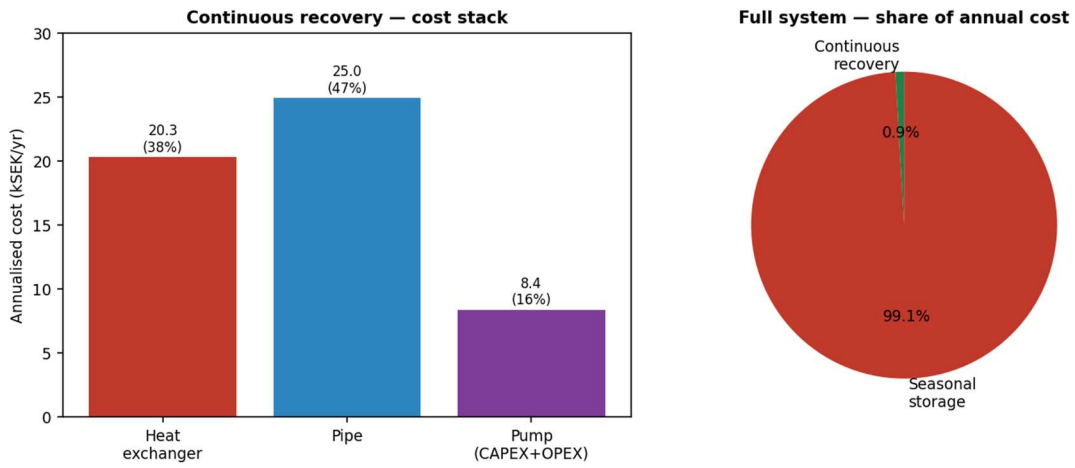

Pipework contributes 46.5 %, heat exchangers 37.9 %, and the pumps 15.6 % within the continuous heat stream integration to DHN network.

Seasonal storage

Including the cavern changes the cost structure entirely. The storage accounts for 99.1 % of full-system annual cost as evident in the pie-chart (figure 6.14). Evaluated alone, the store returns a viability ratio of 1.22. Combining it with the continuous recovery, so that the very cheap heat is credited against the expensive storage infrastructure, brings the full-system R value to 1.04 as evident in the bar chart below (fig 6.15). The full system therefore sits within four per cent of its viability threshold, and the case must be read as partially viable rather than as clearly unviable.

Fig 6.15. *Viability ratio under the three scenarios, Case 4 (log scale; R < 1 is viable).*

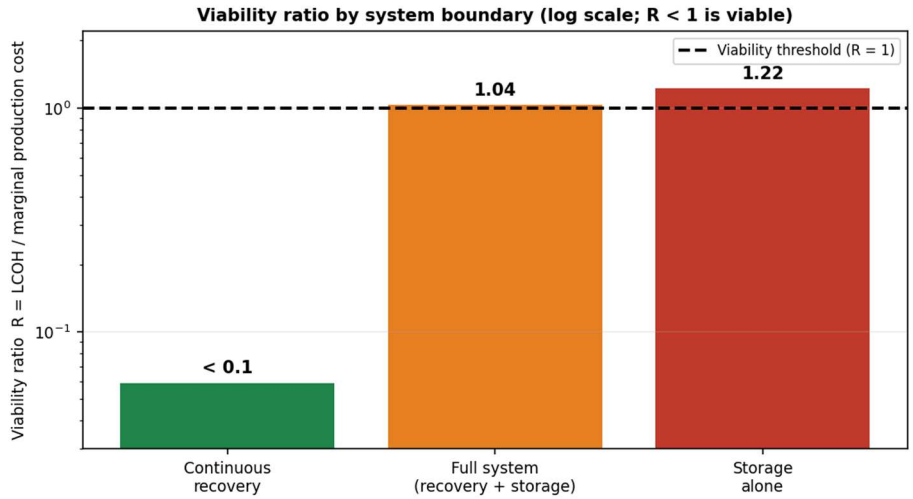

Table 6.17. *Levelised cost summary by system boundary, Case 4.*

System boundary	Annual heat (MWh/yr)	Viability ratio R	Verdict
Continuous recovery (HS-4 + HS-8 + HS-9)	4,540	< 0.1	Clearly viable
Full system (recovery + storage)	28,411	1.04	Marginal, just above threshold
Storage alone	23,871	1.22	Above threshold

A breakeven sweep on the cavern capital cost, holding all other parameters at baseline, places the threshold at approximately 97 % of the quoted budget for the full system, and approximately 82 % for the storage boundary evaluated alone. In other words, the cavern scheme would need to be delivered roughly three per cent under its budgeted cost for the combined project to clear the viability benchmark. That is well within the uncertainty of any construction cost estimate at this stage.

6.4.6 Sensitivity and uncertainty

Table 6.18. *Tornado sensitivity ranges tested, Case 4.*

Parameter	Range tested
Cavern capital cost	±15 %
Recovered surplus volume	±15 %
Continuous waste heat quantity	±15 %
Heat exchanger CAPEX	±15 %
Pipe CAPEX coefficient	±15 %
Pipe length	±15 %
EUR/SEK exchange rate	±15 %
Electricity price	±15 %
Pump efficiency	±15 %

Fig 6.16. *Tornado sensitivity analysis for full-system viability ratio, Case 4.*

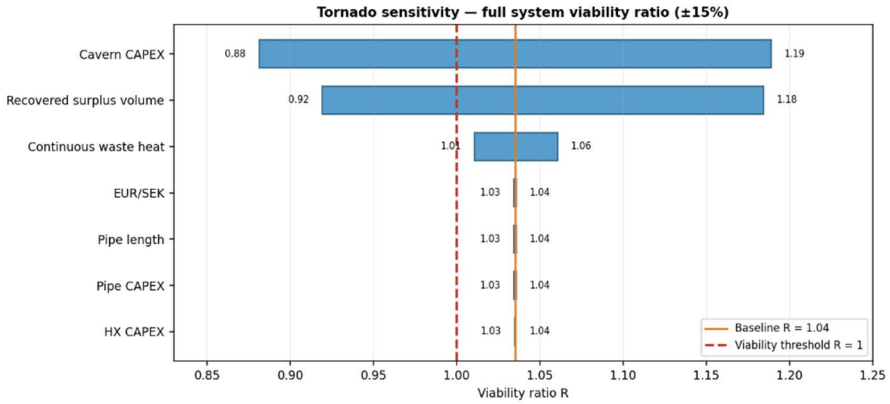

Table 6.18 represents the ranges of the variables tested for sensitivity analysis. The red dotted line represents the viability threshold, R value below this benchmark would make the project viable. Cavern capital cost is the dominant sensitivity, producing a swing of 29.7% and moving the viability ratio between 0.88 and 1.19. Recovered surplus volume from the cooling tower follows closely at 25.6%, spanning 0.92 to 1.18. Continuous waste heat quantity contributes to 12% variation. Every remaining parameter, including the heat exchanger and pipework costs that govern the continuous system entirely, moves the full-system result by 10% or less.

The significant feature is that the two leading parameters each cross the viability threshold on their own. A cavern cost 15 % below budget, or a recovered volume 15 % above the measured figure, would each independently render the combined project viable. Conversely a 15 % overrun on either would place it clearly outside.

Fig 6.17. *Monte Carlo simulation across 1,000 scenarios, Case 4: continuous recovery (left) and full system (right).*

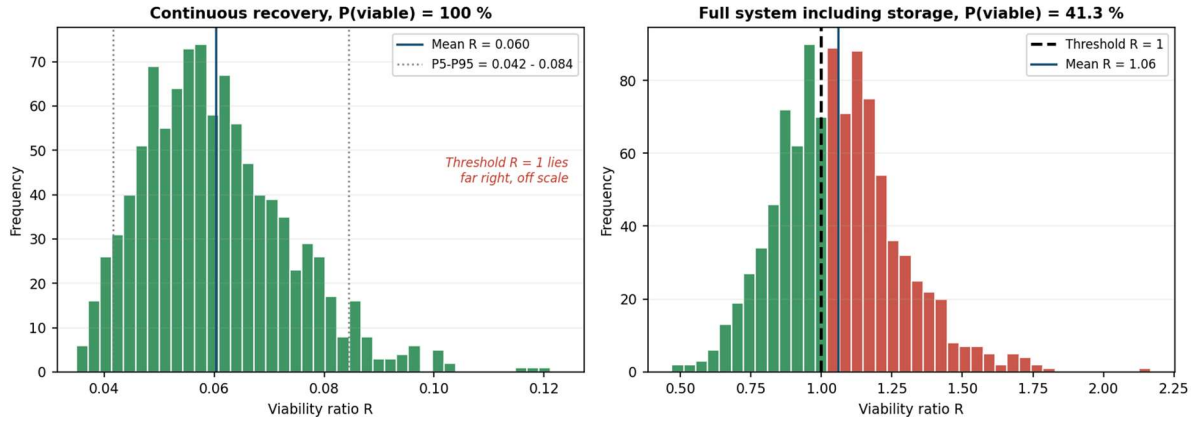

The Monte Carlo simulation confirms this reading. For the continuous recovery the probability of viability is 100 %, with the entire sampled distribution lying an order of magnitude below the threshold with the threshold lying far right off scale in the above fig 6.17 left side plot. For the full system including storage the probability of viability is 41.3 %. The combined project is marginally more likely to fall short of its benchmark than to clear it, but the analysis cannot distinguish the two outcomes with confidence.

6.4.7 Plant efficiency improvement

The second evaluation metric defined in Section 5.9 applies only to this case. Because the recovered streams add useful output without any corresponding increase in fuel input, their effect can be expressed as an improvement in the plant's efficiency. Two figures are reported, corresponding to the two groups of streams.

The fuel input is 69.44 MW, calculated from a waste throughput of 25 t/h at a lower heating value of 10 MJ/kg, giving a design useful output of 64.58 MW at the stated efficiency of 0.93.

Continuous streams only

The three auxiliary streams contribute a combined 658 kW. Applying equation 5.38, the efficiency rises from 0.9300 to 0.9395, an improvement of 0.95 percentage points at no additional fuel cost.

Continuous streams and seasonal storage combined

The recovered summer surplus of 23,871 MWh/yr, expressed as an annual average over the 8,013 operating hours, contributes a further 2.979 MW. Including it increases the efficiency from 0.9300 to 0.9824, an improvement of 5.24 percentage points.

Fig 6.18. *Plant efficiency improvement, Case 4.*

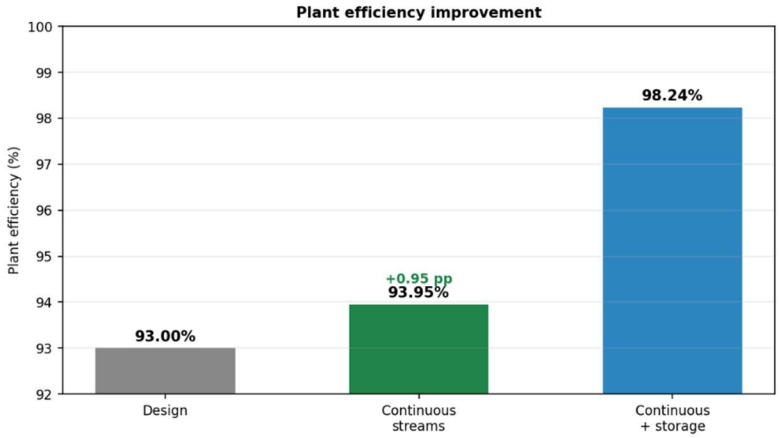

Table 6.19. *Efficiency improvement, Case 4.*

Configuration	Recovered duty	Efficiency	Improvement
Design	—	0.9300	—
Continuous streams (HS-4 + HS-8 + HS-9)	0.658 MW	0.9395	+0.95 pp
Continuous streams + seasonal storage	3.637 MW	0.9824	+5.24 pp

The seasonal storage of heat rejected from cooling tower contributes 4.29 of the 5.24 percentage points.

Table 6.20. *Sensitivity of the efficiency improvement to fuel lower heating value.*

LHV (MJ/kg)	Fuel input (MW)	Continuous only	Combined
9.5	65.97	0.9400 (+1.00 pp)	0.9851 (+5.51 pp)
10.0	69.44	0.9395 (+0.95 pp)	0.9824 (+5.24 pp)
10.5	72.92	0.9390 (+0.90 pp)	0.9799 (+4.99 pp)
11.0	76.39	0.9386 (+0.86 pp)	0.9776 (+4.76 pp)

A sensitivity analysis of efficiency improvement was carried by testing the range of lower heating value provided by the plant (9.5 – 11 MJ/kg). Efficiency improvements scale inversely with the assumed lower heating value, since a lower calorific fuel implies a smaller denominator for the same recovered duty. Across the plausible range for Swedish municipal solid waste the efficiency improvement from continuous streams varies between 0.86 and 1.00 percentage points and the combined streams improvement between 4.76 and 5.51 points. Neither range is wide enough for the conclusion to change.

6.4.8 Discussion

The continuous streams including the soot blower drain, chiller condenser heat and compressor aftercooler are clearly viable at an R value far below 1, while the seasonal storage of cooling tower rejection sits marginally above the threshold at 1.06.

The continuous recovery succeeds because the transport question that governs our first three cases effectively disappears. The three streams deliver 4,540 MWh/yr across a combined connection length of 35 m for a total installed capital cost of 724 kSEK. Where ICA Maxi failed because a small source could not support a long connection. Here a comparably modest source needs much smaller connection infrastructure. The result is a levelised cost an order of magnitude below the benchmark and a plant efficiency improvement of 0.95 percentage points at no fuel cost.

The seasonal storage result is more finely balanced than the continuous recovery, sitting four per cent above its viability threshold. The Monte Carlo probability of 41.3 % means the case is genuinely undecided on the evidence considered here, and two further factors, not included in this analysis, could tip it toward viability. First, the value of storage itself. Having stored heat available in winter can reduce the need to run the oil or electric boiler, a benefit not captured by simply costing the heat delivered. Since the electric boiler runs only when electricity is cheap or negative priced, there is uncertainty around exactly when the storage discharge would substitute the electric boiler operation. Second, the analysis only counts the heat the store sends back to the network; it does not credit the store for reducing cooling tower operation. Establishing any of these would require an investment analysis at plant level rather than a levelised cost comparison at stream level.

The compressor aftercooler stream also suggests a further improvement worth noting. Switching from air to water cooling would raise the heat transfer coefficient by roughly two orders of magnitude, allowing a much larger share of the compressor's rejected heat to be recovered economically. Since this stream already runs at the highest source temperature of the four identified, retrofitting a water-cooled aftercooler is a plausible route to a materially larger and cheaper recovery from HS-8, and is worth investigating directly with the plant's compressor supplier.

Read together, the two scenarios give the transferable finding of this case. The continuous streams are the smaller prize, accounting for 0.95 of the 5.24 percentage point potential efficiency improvement, yet they are worth recovering especially considering its remarkable economic viability. The summer surplus is five times larger in energy terms and carries the remaining 4.29 percentage points, yet its economics cannot be settled here. This reinforces the pattern established across the three earlier cases. Distance, storage and the quantity of available waste heat are the terms that predominantly decide these projects.

7. Conclusions and Further Work

This chapter draws together the results of the four cases, answers the research questions set out in Section 3.2, and identifies the future work that would need to follow to resolve the questions this thesis leaves open.

7.1 Answers to the research questions

All four integrations proved technically feasible to size, and the sizes themselves span a range worth stating plainly. Heat exchanger area ranged from 5.83 m² at ICA Maxi to 468 m² at Metsä Board, connection pipe from DN25 over 3500 km for ICA Maxi case to DN150 over 160 m at in case of Asta Real, and circulation pump duty from 1 kW to 192 kW. The required infrastructure is overwhelmingly dictated by source temperature and temporal availability. Low-grade sources require heat pumps with floating condenser controls, while intermittent sources necessitate seasonal thermal energy storage (TES). The thermodynamic sophistication of heat pumps and heat exchangers, however, contributes minimally to the total system economics compared to the sheer scale of transmission pipes and storage sizes required.

Another interesting finding from the sizing work is that the heat transfer medium of the cooling streams matters more than the duty. The compressor aftercooler in Case 4 carries under three per cent of that plant's continuous heat but demands 27 per cent of its installed exchanger area, because the gas-to-liquid heat transfer coefficient is roughly one-hundredth the liquid-to-liquid value.

Viability is not guaranteed simply because waste heat is available. Case 1 (ICA Maxi) proved highly unviable, with an LCOH of 4,836 SEK/MWh against a benchmark of 347 SEK/MWh, driven entirely by the capital expenditure of a 3,500 m connection pipe. Case 2 (AstaReal) also proved unviable, despite a 160 m connection and a levelised cost of just 22 SEK/MWh excluding storage, the 128,775 m³ seasonal store lifted the total to 364 SEK/MWh against the same 347 SEK/MWh benchmark. Case 3 (Metsä Board), by contrast, proved comfortably viable at 231 SEK/MWh against 263.2 SEK/MWh, because its 531,459 m³ store is spread across 98 GWh/yr of delivered heat rather than 14.7 GWh/yr. The decisive variable is therefore not connection distance alone but delivered volume as well. It really determines whether a seasonal store can be afforded at all.

Table 7.1. *Summary of results across the four cases.*

Metric	Case 1: ICA Maxi	Case 2: AstaReal	Case 3: Metsä Board	Case 4: WtE plant
Levelised cost	4,836 SEK/MWh	364 SEK/MWh	231 SEK/MWh	11.8 SEK/MWh (continuous)
Benchmark	347 SEK/MWh	347 SEK/MWh	263.2 SEK/MWh	Confidential (ratio R)
Margin	≈14× above	1.05× above	1.14x below	R < 0.1 continuous; R = 1.04 full system
P(viable)	0.0 %	21.2 %	87.3 %	100 % continuous; 41.3 % full system
Connection distance	3,500 m	160 m	900 m	35 m combined

Verdict	Not viable	Not Viable	Viable	Marginal

Turning the methodology inward in Case 4 (Waste-to-Energy Plant) revealed the most economically compelling integration. Bypassing long transmission lines allowed continuous auxiliary streams to be recovered at an exceptionally low LCOH of 11.8 SEK/MWh, yielding a 0.95 percentage point improvement in overall plant boiler efficiency at no additional fuel cost. When factoring in seasonal storage for summer cooling-tower rejection, the efficiency improvement jumped to 5.24 percentage points, though the high capital cost of rock cavern storage pushed the full system to the very edge of economic viability (viability ratio of 1.04).

7.2 The breakeven distance as a screening tool

Sweeping pipe length while holding all other parameters at baseline gives the distance at which levelised cost crosses the marginal production cost: roughly 90 m for ICA Maxi and 1.95 km for Metsä Board. This turns a single project result into a reusable rule of thumb on how close a particular type of source of a given size and temperature would need to be to the network to be worth connecting. The ICA Maxi result for instance illustrates this well. Since supermarkets of similar size and refrigeration load reject waste heat at a comparable rate and temperature, the 90 m breakeven can be used to pre-screen other ICA Maxi stores of similar size across the country purely on their distance to the nearest district heating main, without resizing the connection for each one individually.

7.3 Further work

In the storage-dominated case 4, the store is credited only with the heat it returns to the network. It is not credited with avoided cooling tower operation, with displaced oil or electric boiler dispatch during the winter discharge season, or with the scheduling flexibility a large store compliments on plant operation. A plant-level investment analysis rather than a stream-level levelised cost comparison would capture these, and would improve the probability of viability further for case 4 combined case.

Asta Real, Metsä Board and Case 4 require large storage dominating the project costs. Using the receiving network's other generation assets to absorb the seasonal mismatch may be a cheaper route to the same outcome. Establishing this would require the host network to be modelled at system level, which is outside the boundary adopted here but is a natural extension of it.

Switching the HS-8 stream for the compressor aftercooler from air to water cooling would raise the heat transfer coefficient by roughly two orders of magnitude, allowing a considerably larger share of the compressor's rejected heat to be recovered economically. Since this stream already runs at the highest source temperature of the four identified continuous streams in Case 4, this is worth pursuing directly with the plant's compressor supplier.

The framework developed here applies one consistent method to four cases. Applying it across a larger population of sources would allow the breakeven distance to be expressed as a function of annual heat

volume, seasonal variation and source temperature rather than tabulated case by case, which would turn it from a per-project result into a genuine screening tool.

References

Adrianto, L., et al. (2018). CO_2 Refrigeration to District Heating Network — Scenario Analysis. Master's thesis project, KTH Royal Institute of Technology, Stockholm.

Akar, S., Oh, H., Beckers, K., Vivas, C. and Salehi, S. (2023) Techno-Economic Analysis for a Potential Geothermal District Heating System in Tuttle, Oklahoma: Preprint. Golden, CO: National Renewable Energy Laboratory. NREL/CP-5700-86946

Averfalk, H. and Werner, S. (2017) 'Essential improvements in future district heating systems', Energy Procedia, 137, pp. 639–649.

Averfalk, H., Ingvarsson, P., Persson, U., Gong, M. and Werner, S. (2017) 'Large heat pumps in Swedish district heating systems', Renewable and Sustainable Energy Reviews, 79, pp. 1275–1284.

Baeuerle, Y.I., Arpagaus, C. and Haller, M.Y. (2025) 'A review of seasonal energy storage for net-zero industrial heat: thermal and power-to-X storage including the novel concept of renewable metal energy carriers', Energies, 18(9),, p. 2204.

Bergman, T.L., Lavine, A.S., Incropera, F.P. and DeWitt, D.P. (2011) Fundamentals of heat and mass transfer. 7th edn. Hoboken, NJ: John Wiley and Sons.

Bocchio, E. and Elahi, A. (2017). Waste-to-energy plants with low temperature heat recovery via flue gas condensation and heat pumps. Master's thesis, Politecnico di Milano.

Bolaji, B.O. and Huan, Z. (2013). 'Ozone depletion and global warming: Case for the use of natural refrigerant – a review', Renewable and Sustainable Energy Reviews, 18,, pp. 49–54.

Broberg, S., Backlund, S., Karlsson, M. and Thollander, P. (2012). 'Industrial excess heat deliveries to Swedish district heating networks: Drop it like it's hot', Energy Policy, 51,, pp. 332–339.

Brückner, S., Liu, S., Miró, L., Radspieler, M., Cabeza, L.F. and Lävemann, E. (2015). 'Industrial waste heat recovery technologies: An economic analysis of heat transformation technologies', Applied Energy, 151,, pp. 157–167

Bühler, F., Petrović, S., Karlsson, K. and Elmegaard, B. (2018). 'Spatiotemporal and economic analysis of industrial excess heat as a resource for district heating', Energy, 151,, pp. 715–728.

Connolly, D., Lund, H., Mathiesen, B. V., Werner, S., Möller, B., Persson, U., Boermans, T., Trier, D., Østergaard, P. A., and Nielsen, S. (2014). Heat Roadmap Europe: Combining district heating with heat savings to decarbonise the EU energy system. Energy Policy, 65, 475–489.

Danish Energy Agency (2026). Technology Data for Generation of Electricity and District Heating. Copenhagen: Danish Energy Agency. Available at: https://ens.dk/en/analyses-and-statistics/technology-data-generation-electricity-and-district-

heating(https://ens.dk/en/analyses-and-statistics/technology-data-generation-electricity-and-district-heating)

Danish Energy Agency (DEA) (2023). Technology Data for Energy Plants: Generation of Electricity and District Heating. Copenhagen, Denmark.

Danish Energy Agency (DEA) and Energinet (2018) Technology Data – Energy Storage. ISBN 978-87-93902-46-1. Copenhagen: Danish Energy Agency, Carsten Niebuhrs Gade 43.

Dorotić, H., Čuljak, K., Miškić, J., Pukšec, T. and Duić, N. (2019). 'Technical and Economic Assessment of Supermarket and Power Substation Waste Heat Integration into Existing District Heating Systems', Energies, 12(9), 1734.

Energiforsk (2022). Prosumption Toolbox for District Heating — Methodology for Evaluating Third-Party Heat Supply. Energiforsk AB, Stockholm.

Engineering ToolBox (2003) Heat Exchangers — Overall Heat Transfer Coefficients. Available at: https://www.engineeringtoolbox.com/heat-transfer-coefficients-exchangers-d_450.html(https://www.engineeringtoolbox.com/heat-transfer-coefficients-exchangers-d_450.html)

European Commission (2021). Communication from the Commission to the European Parliament, the Council, the European Economic and Social Committee and the Committee of the Regions: 'Fit for 55': delivering the EU's 2030 Climate Target on the way to climate neutrality. COM(2021) 550 final. Brussels: European Commission

European Parliament and Council of the European Union (2023). Directive (EU) 2023/1791 of the European Parliament and of the Council of 13 September 2023 on energy efficiency and amending Regulation (EU) 2023/955 (recast). Official Journal of the European Union, L 231,, pp. 1–111.

Eurostat (2024). Energy consumption in households - Statistics Explained. European Commission. Available at:https://ec.europa.eu/eurostat/statistics-explained/index.php?title=Energy_consumption_in_households(https://ec.europa.eu/eurostat/statistics-explained/index.php?title=Energy_consumption_in_households)

Frederiksen, S. and Werner, S. (2013). District Heating and Cooling. Studentlitteratur, Lund, Sweden.

Fricke, B. A. (2011). Heat rejection from supermarket refrigeration systems. ASHRAE Transactions, 117(2).

Holmberg, H., Tuomaala, M., Haikonen, T., and Ahtila, P. (2012). Allocation of fuel costs and CO_2-emissions to heat and power in an industrial CHP plant. Applied Energy, 93, 614–623.

Hotmaps (2024). The Hotmaps Project — Open Source Heating and Cooling Mapping and Planning Toolbox. Available at: https://www.hotmaps.eu. Accessed 2026.

How algae cultivation benefits from heating households. Updated 7 March 2024. Available at: https://energyplaza.vattenfall.se/blogg/sa-tjanar-algodlingen-pa-att-varma-hushall-i-gustavsberg(https://energyplaza.vattenfall.se/blogg/sa-tjanar-algodlingen-pa-att-varma-hushall-i-gustavsberg) (Accessed 2026)

IEA District Heating and Cooling Programme (IEA DHC) (2021). Annex TS3: Hybrid Energy Networks (District Heating and Cooling, Power, Gas). Final Report. International Energy Agency.

Incropera, F. P., DeWitt, D. P., Bergman, T. L., and Lavine, A. S. (2007). Fundamentals of Heat and Mass Transfer (6th ed.). John Wiley and Sons, Hoboken, NJ.

Jouhara, H., Khordehgah, N., Almahmoud, S., Delpech, B., Chauhan, A. and Tassou, S.A. (2018). 'Waste heat recovery technologies and applications', Thermal Science and Engineering Progress, 6,, pp. 268–289.

Karner, K., McKenna, R., Klobasa, M., Kienberger, T., and Posch, A. (2018). Industrial excess heat recovery in industry-city networks: a technical, environmental and economic assessment of heat flexibility. Journal of Cleaner Production, 193, 771–783.

Kumar, A., Somanna, A., Thakur, J., and Gunasekara, S. (2025). Business model evaluation for industrial waste heat utilisation: comparison of district heating integration, organic Rankine cycle, and steam export pathways. In collaboration with Ramboll Sweden.

Kumar, S., Kök, A., Dalgren, J., Thakur, J., Martin, V. and Gardumi, F. (2025). 'Strategic integration of urban excess heat sources in a district heating system: A Spatio-temporal optimisation methodology', Applied Energy, 396, 126236.

Lund, H., Werner, S., Wiltshire, R., Svendsen, S., Thorsen, J. E., Hvelplund, F., and Mathiesen, B. V. (2014). 4th Generation District Heating (4GDH): Integrating smart thermal grids into future sustainable energy systems. Energy, 68, 1–11.

Lygnerud, K. and Werner, S. (2018). Risk assessment of industrial excess heat recovery in district heating systems. Energy, 151, 430–441.

Lygnerud, K., Ottosson, J., Kensby, J., and Johansson, L. (2021). Business models combining heat pumps and district heating in buildings generate cost and emission savings. Energy, 234, 121260.

Mathiesen, B. V., Lund, H., Connolly, D., Wenzel, H., Østergaard, P. A., Möller, B., Nielsen, S., Ridjan, I., Karnøe, P., Sperling, K., and Hvelplund, F. K. (2015). Smart Energy Systems for coherent 100% renewable energy and transport solutions. Applied Energy, 145, 139–154.

Nils Holgersson Group (2025). Annual Report on District Heating Prices in Swedish Municipalities. Available via the Nils Holgersson website.

Nils Holgersson-gruppen (2023). Fjärrvärme 2023 - Nils Holgersson-rapporten. Available at: https://nilsholgersson.nu/rapporter/rapport-2023/fjarrvarme-2023/(https://nilsholgersson.nu/rapporter/rapport-2023/fjarrvarme-2023/)

Nils Holgersson-gruppen (2024). Fjärrvärme 2024 - Nils Holgersson-rapporten. Available at: https://nilsholgersson.nu/rapporter/rapport-2024/fjarrvarme-2024/(https://nilsholgersson.nu/rapporter/rapport-2024/fjarrvarme-2024/)

nPro Technologies (2024). District Heating Pipe Cost Estimation Tool. Available at: https://www.npro.energy.

Olofsson, J. and Berntsson, T. (2020). Operating strategies for kraft pulp mills with integrated combined heat and power: assessment of waste heat utilisation potential. Energies, 13(9), 2413.

Packaging Gateway (2023) Metsa Board's board and pulp mill expansion. Available at: https://www.packaging-gateway.com/projects/metsa-boards-and-pulp-mill-expansion/(https://www.packaging-gateway.com/projects/metsa-boards-and-pulp-mill-expansion/)

Persson, U. and Werner, S. (2011). Heat distribution and the future competitiveness of district heating. Applied Energy, 88(3), 568–576.

Persson, U. and Werner, S. (2012) 'District heating in sequential energy supply', Applied Energy, 95, pp. 123–131.

Persson, U. and Werner, S. (2012), Renewable Energy, 45, pp. 196–207.

Pieper, H., Ommen, T., Buhler, F., Lava Paaske, B., Elmegaard, B., and Markussen, W. B. (2018). Allocation of investment costs for large-scale heat pumps supplying district heating. Energy Procedia, 147, 358–367.

Pumps and Systems (2020) How to Define and Measure Centrifugal Pump Efficiency: Part 1. Available at: https://www.pumpsandsystems.com/how-define-measure-centrifugal-pump-efficiency-part-1(https://www.pumpsandsystems.com/how-define-measure-centrifugal-pump-efficiency-part-1)

Renström, J. and Ludvig, K. (2025). Excess Heat in Sweden: Mapping of potential, challenges and opportunities. Mölndal: Profu.

Roquet, M. (2024). Technoeconomic Analysis of District Heating Pipe Sizing. Master's thesis.

S&P Global Ratings (2024). Credit FAQ: How Rising Fuel Costs Could Stress Swedish District Heating Companies' Creditworthiness. Available at: https://www.spglobal.com/ratings/en/regulatory/article/240212-credit-faq-how-rising-fuel-costs-could-stress-swedish-district-heating-companies-creditworthiness-s12878251(https://www.spglobal.com/ratings/en/regulatory/article/240212-credit-faq-how-rising-fuel-costs-could-stress-swedish-district-heating-companies-creditworthiness-s12878251)

Sadowski, D., Piaskowska-Silarska, M. and Piaskowski, W. (2022) 'Efficiency of a Compressor Heat Pump System in Different Cycle Designs: A Simulation Study for Low-Enthalpy Geothermal Resources', Energies, 15(15), 5546.

Schmidt, T. and Sørensen, P. A. (2018). Monitoring results from large scale heat storages for district heating in Denmark. In Proceedings of the 14th International Conference on Energy Storage (EnerSTOCK 2018), Adana, Turkey.

Selinder, P. (2026) Personal communication with the author, Vattenfall.

Shah, R. K. and Sekulić, D. P. (2003). Fundamentals of Heat Exchanger Design. John Wiley and Sons, Hoboken, NJ.

Sjödin, J. and Henning, D. (2004). Calculating the marginal costs of a district heating utility. Applied Energy, 78(1), 1–18.

Slegers, P. M., Lösing, M. B., Wijffels, R. H., van Straten, G., and van Boxtel, A. J. B. (2013). Scenario evaluation of open pond microalgae production. Algal Research, 2(4), 358–368.

SMHI (2025). Swedish Meteorological and Hydrological Institute, Open Data Portal. Station 98230 (Stockholm-Observatoriekullen) and station 138240 (Örnsköldsvik Flygplats). Available at: https://www.smhi.se/data.

Thanasoulas, I., et al. (2023). Investigating the heating and air conditioning provision capability of a supermarket to neighbouring buildings. Applied Thermal Engineering.

Vattenfall Värme AB (2024). Prisändringsmodell — Haninge, Tyresö, Älta och Gustavsberg. Customer tariff notification. Vattenfall Värme AB, Stockholm.

Vlcan, F. (2025). Assessing the Feasibility and Viability of Industrial Waste Heat Utilization for District Heating in Oskarshamn: A Techno-Economic Perspective. Master's thesis project, KTH Royal Institute of Technology.

Wahlroos, M., Pärssinen, M., Manner, J., and Syri, S. (2018). Future views on waste heat utilization — Case of data centers in Northern Europe. Renewable and Sustainable Energy Reviews, 82, 1749–1764.

Werner, S. (2017). 'District heating and cooling in Sweden', Energy, 126,, pp. 419-429.

Werner, S. (2017). International review of district heating and cooling. Energy, 137, 617–631.

Winkler cited in FVB (2025) World-class energy storage – Mälarenergi leads the way. Available at: https://www.fvb.se/en/fvb-nytt/world-class-energy-storage-malarenergi-leads-the-way/(https://www.fvb.se/en/fvb-nytt/world-class-energy-storage-malarenergi-leads-the-way/)

Övik Energi (2026) Övik Energis prisändringsmodell för år 2026–2028 för fjärrvärme till näringsfastigheter. Örnsköldsvik: Övik Energi AB.